1-1-2016

Enhancement Of Cancer Vaccine Efficacy Via Nanoparticle Or Molecular-Based Adjuvants

Myunggi An
Wayne State University,

ENHANCEMENT OF CANCER VACCINE EFFICACY VIA NANOPARTICLE OR MOLECULAR-BASED ADJUVANTS

by

MYUNGGI AN

DISSERTATION

Submitted to the Graduate School

of Wayne State University,

Detroit, Michigan

in partial fulfillment of the requirements

for the degree of

MASTER OF SCIENCE

2016

MAJOR: MATERIALS SCIENCE AND

ENGINEERING

Approved by:

_____

Advisor Date

ACKNOWLEDGEMENTS

I would like to thank my thesis advisor, Dr. Haipeng Liu, for your constant support of my work and for your immeasurable patience with me and optimism for my results. I would also like to thank you for teaching the hard work of animal experiments. It was a luxury to be able to concentrate solely on the research. You continued to provide mentorship and provided me endless encouraging not to give up my project. Thank you for allowing me to find my way and to spend time until I complete my long term project. Without your guidance and persistent help, this thesis would not have been possible. I really do not know how to convey how much I appreciate your patience, your teaching, and your kindness; truly thank you for taking me onboard!

I would like to thank my committee members, Dr. Guangzhao Mao and Dr. Zhiqiang Cao for contributing their time and expertise to help mold and strengthen the work presented in this dissertation.

Chunsong and Jingchao, thank you for being my good friend, for listening to me, and for your mentorship throughout the whole process. Your cheerful optimism and insights for trouble-shooting in the lab helped direct my project. I will miss the moment that we got animal training, worked to complete the complicated experiments, and played the tennis together. Thank you for questioning me, and for the years of hard work that are now summed up in this thesis.

Dr. Li and Dr. Yang, I want to extend a huge thank you for providing your teaching, and your kindness. Your thoughtful scientific analysis were huge assets to my project and your encouragement in my graduate study were immensely helpful.

It is impossible to fully thank my family for all of their love and support of the years. Thank you for always expecting the best out of me, for answering when I call, and so many more thing. I also need to thank your steadfast belief in me and for encouraging me to pursue my goal.

TABLE OF CONTENTS

Acknowledgments i

List of Figures vi

Chapter 1. Background and scope of thesis 1

1.1. Necessity of vaccine adjuvant development 1

1.2. Scope and outline of thesis 5

Chapter 2. Lipid coated silica nanoparticles as a pathogen mimicking platform for lymph node targeting 6

2.1. Introduction 6

2.2. Materials and Method 8

*2.2.*1. Preparation of CpG ODN loaded SiNPs (CS) and lipid-coated SiNPs (LCS) 8

2.2.2. Size and zeta potential measurements 9

2.2.3. *In vitro* characterization 9

2.2.4. Analysis of cellular uptake 10

2.2.5. *In vivo* lymph node targeting 10

2.2.6. Immunization 11

2.2.7. Tumor model 12

2.2.8. Statistical analysis 12

2.3. Results and discussion 12

2.3.1. Design of LN-targeting CpG loaded SiNPs 12

2.3.2. SiNPs formulation efficiently targets CpG to the LN 17

2.3.3. Design of LN-targeting lipid coated SiNPs and pathogen mimicking composite materials 21

2.3.4. Lipid coated SiNPs formulation efficiently targets CpG to the LN 25
2.3.5. SiNPs enhances cellular uptake and immune stimulation of CpG *in vitro* 28
2.3.6. SiNPs formulations trigger potent antigen-specific immune responses 30
2.3.7. SiNPs vaccination elicit a protective anti-tumor immune response 35
2.4. Conclusions 36
Chapter 3. Dissolving microneedle arrays for transdermal delivery of molecular vaccines .38
3.1. Introduction 38
3.2. Background 40
3.3. Materials and Method 41
3.3.1. DNA synthesis and lipophilic conjugation 41
3.3.2. Synthesis of peptide amphiphile 42
3.3.3. Purification of synthesized DNA 42
3.3.4. Design and preparation of microneedle arrays (MNs) 43
3.3.5. Characterization of MNs 44
3.3.6. *In vivo* MNs application and vaccine release 45
3.3.7. Immunization 45
3.3.8. Statistical analysis 47
3.4. Results and discussion 47
3.4.1. Preparation of MNs 47
3.4.2. Insertion and dissolution of MNs in skin 48
3.4.3. MNs vaccination 50
3.5. Conclusions 55
4. Chapter 4. Conclusion and future work 56

References 58

Abstract 71

Autobiographical Statement 72

LIST OF FIGURES

Figure 1-1. Cancer-Immunity Cycle. 3

Figure 2-1. CpG ODN coated silica nanoparticles preparations and kinetics of CpG ODN from nanoparticles. 15

Figure 2-2. Characterizations of nanoparticles and expected debye screening length. 17

Figure 2-3. *In vivo* nanoparticle delivery to draining lymph nodes measured at 24 h. 19

Figure 2-4. *In vivo* nanoparticle delivery to draining lymph nodes measured at 30 h. 21

Figure 2-5. Preparation of lipid coated nanoparticles. 23

Figure 2-6. Preparation of pathogen mimicking composite nanoparticle. 24

Figure 2-7. Transmission electron microscopy images of nanoparticles. 25

Figure 2-8. *In vivo* lipid coated nanoparticle delivery to draining lymph nodes. 26

Figure 2-9. Immunohistochemistry of inguinal lymph nodes. 27

Figure 2-10. *In vitro* nanoparticle delivery and its FACS analysis. 28

Figure 2-11. Alkaline phosphatase activity of nanoparticle from toll like receptor 9 cells. .. 30

Figure 2-12. Antigen specific immunogenicity vaccinated by lipid coated nanoparticles. ... 32

Figure 2-13. Antibody responses in mice sera immunized by lipid coated nanoparticles. 34

Figure 2-14. Lipid coated nanoparticle vaccination hinder cancer progression and enhances mice survival. 36

Figure 3-1. Structure of diacyl lipid conjugated CpG ODN (Lipo-G_2-CpG). 42

Figure 3-2. Preparation of Amphiphilic OVA-II peptide (DSPE-PEG-OVA-II). 42

Figure 3-3. Schematic diagram of microneedle arrays fabrication. 44

Figure 3-4. Time table of mice Immunization via intradermal injections or microneedle delivery. 46

Figure 3-5. Characterization of microneedle arrays before and after applications. 48

Figure 3-6. *In vivo* characterization of vaccine release from microneedle arrays. 49

Figure 3-7.OVA specific immunogenicity vaccinated via microneedle delivery. 51

Figure 3-8. OVA-II specific immunogenicity vaccinated via microneedle delivery. 52

Figure 3-9. Antibody responses in mice sera immunized via microneedle delivery. 53

Figure 3-10. Schematic diagram of transdermal delivery of albumin hitchhiking molecular vaccine. 54

1. Background and scope of thesis

1.1. Necessity of vaccine adjuvant development

In 2005, 7.6 million people died by cancer out of 58 million deaths worldwide.[1, 2] Based on projections, cancer deaths will continue to increase with an estimated 9 million people dying from cancer in 2015, and 11.4 million in 2030 (World Health Organization, 2006a). Cancer can be treated by surgery, chemotherapy, radiation therapy and immunotherapy.[3, 4] Complete elimination of the tumor without damage to the rest of the body would be the ideal aim of treatment. Sometimes this can be achieved by tumor tissue surgery, but the propensity of cancers to spread adjacent tissue by microscopic metastasis often limits its effectiveness. There are side effects associated with chemotherapy and radiotherapy that can have a negative effect on normal cells near the cancer. On the other hand, Immunotherapy has great potential to treat cancer and prevent future relapse by triggering the immune system to recognize and kill cancer cells. A variety of strategies are continuing to evolve in the laboratory and in the clinic, including therapeutic non-cellular (vector-based or subunit) cancer vaccines[4], dendritic cell vaccines[5, 6], engineered T cells[7-9], and immune checkpoint blockade[10-12]. Despite their promising approaches, much more research is needed to address problems in immunology such as how and why certain cancers fail to respond to immunotherapy. The newly emerging field of immune-engineering is exploring some of these challenges, and there is ample opportunities for engineers to contribute their ideas and tools to mediate cancer regression in preclinical and clinical models.[13, 14]

To understand how immunotherapy works, it is necessary to know how the immune system protects our body against disease. Vertebrates are emerged with two complementary immune systems, the innate immune system and the adaptive immune system.[15] The adaptive immune system is equipped with two key weapons: antigen-recognizing lymphocytes, B cells and T

cells, which specifically target the invader, and provide a memory response to prevent a repeat of the infection.[16, 17] The innate immune system, in contrast to the adaptive system, is the first defense line, eliciting inflammatory response at the early stage.[18] To protect the host from succumbing to infections, the innate immune system phagocytoses the pathogen, recruits natural killer cells (NK cells), and maturates dendritic cells. Those innate immune responses are linked to adaptive immune responses following four fundamental tasks. First, innate immune system must rapidly detect any infectious agent, regardless of whether it is a fungus, virus, bacteria, or parasite. Second, innate immune cells need to rapidly categorize the type of invading infectious agent. Third, innate immune defenses eliminate the pathogen or internalize the categorized infectious agents. Fourth, innate immune cells induce the appropriate type of adaptive immune response, thereby eradicating the infection and preventing its recurrence.

The primitive part of innate immune cells that enables them to recognize conserved pathogen seems to be their repertoire of what have been termed pattern-recognition receptors (PRRs), which lead to transcriptional expression of inflammatory mediators that coordinate the elimination of pathogens.[19] The toll-like receptor (TLR) is one of the best-characterized PRR families and 10 types of TLR are known in humans.[20] TLRs that are responsible for sensing molecule's characteristic of extracellular pathogens are expressed on cell surface, whereas TLRs that detect intracellular pathogens are expressed within innate immune cells. For example, TLR9 detects unmethylated CpG dinucleotides, which are relatively common in bacterial DNA.[21, 22]

Most types of immune cells do not express TLR9, and thus are not activated directly by CpG oligonucletodes (ODNs). CpG ODNs only activate cells expressing TLR9 receptors. In mice, plasmacytoid dendritic cells (pDCs) activated through TLR9 create a T_H1-like cytokine milieu by secreting INF-α/β, IL-12, TNF-α. These cytokines are considered to be important

in triggering T_H1 responses, which may explain why administration of mice with this TLR9 ligand gives a higher level of antigen-specific IFN-γ secretion and $CD8^+$ T cells.[13] CpG ODNs enhance the number and function of tumor-specific cytotoxic $CD8^+$ T cells.[23] The T_H1-like cytokine milieu also activate NK cells, secreting IFN-γ and gaining lytic activity. In addition, the B cells turn to more sensitive to activation through their antigen receptor, and both B cells and pDCs can trigger expression of costimulatory molecules, enhancing their ability to activate T cell responses.[15] All of the cellular immune effects of CpG ODNs are thought to result from TLR9- stimulated B cells and pDCs, showing expression of co-stimulatory molecules and co-activation of naive T cells and germinal center or memory B cells through their antigen receptor (Figure 1-1).[24]

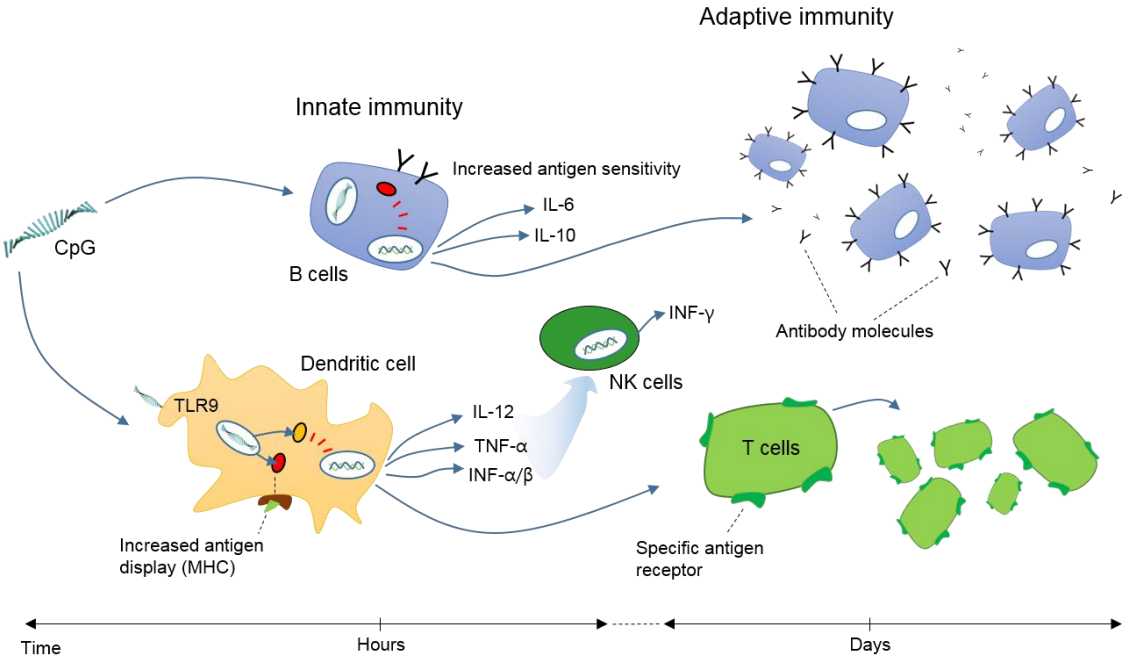

Figure 1-1. CpG cellular mechanism of action.

CpG ODNs are easy to synthesize in the lab and are used as vaccine adjuvants to augment the immune responses (Figure 1-1). To avoid the rapid enzymatic degradation *in vivo*, CpG

ODNs are most often made with a nuclease-resistant phosphorothioate backbone. They are effective for preventing and treating infectious diseases, allergies, and cancers by activating host defense mechanisms which elicit innate and acquired immune responses.[25] Thus, CpG ODNs have been widely used as an effective therapeutic tool to enhance immune responses through the activation of TLR9. However, parenteral administration of unformulated CpG ODNs fails to reach lymph nodes (LNs), the anatomic organ where the primary functions of immune cells are orchestrated. LNs are highly organized structures where the interaction among T cells, B cells, and APCs are hosted in a stromal cell matrix. They are thus central targets in antigen presentation and immune activation.[26] Adjuvants fail to reach the LNs often lead to unacceptable systemic side effects, which have limited the advance of adjuvants in vaccine applications. Thus, approaches that target vaccine components to LNs play key roles in promoting immune activation and have the great potential in transforming disease treatment.

1.2. Scope and outline of thesis

In this thesis, we introduced therapeutic applications of activating TLR9 with synthetic CpG oligodeoxynucleotide (ODN) agonists in nanoparticle or molecular form to activate immune responses in animal models. As a nanoparticle deliver platform, positively charged silica nanoparticles (SiNPs) were explored to load immunomodulators that are capable of targeting the draining LNs (dLNs) and mimicking the size, geometry and surface feathers of live viral pathogens. We next demonstrated the use of microneedles arrays as a transdermal delivery platform prepared by a water-soluble polymer to release molecular vaccines in epidermis and target them to draining lymph nodes.

Chapter 2 describes lipid coated SiNPs for targeting CpG DNA to dLNs. Immunization with nanoparticles showed potent cellular and humoral immunity superior to vaccination with soluble CpG ODNs. We systematically characterized electrostatic charge interactions between SiNPs and CpG ODNs, and explored the optimum loading ratio of CpG ODNs on SiNPs, which lead to high colloidal stability with enhanced lymphatic uptakes. We then compared immunogenicity profiles of nanoparticle and soluble CpG ODN in vaccination.

In Chapter 3 we explored the transdermal delivery platform using dissolving microneedle arrays (MNs), which can penetrate the skin and facilitate the rapid release of vaccine components in epidermis. We combined this strategy with an albumin ‘hitchhiking’ approach that can promote interaction with and uptake across the lymphatic endothelium. Vaccination via MNs generated robust immune responses, showing enhanced T cell and antibody responses. We characterized the morphology and vaccine loading capabilities of MNs, and systematically explored how the transdermal delivery of molecular vaccines impacted cellular and humoral immunities.

Chapter 4 is the conclusion and future work.

2. Lipid coated silica nanoparticles as a pathogen mimicking platform for lymph node targeting

2.1. Introduction

Vaccination is to stimulate the immune system by administration of antigenic materials in order to develop adaptive immunity to diseases. It represents the single most effective medical intervention in modern medicine. Traditionally, attenuated live or killed whole pathogens were administrated into human body to trigger protective immune responses without causing illness. Recent advances in immunology have led to the development of more defined synthetic subunit antigens (proteins, peptides or nucleic acids) to improve vaccine stability, safety and tolerability. More importantly, subunit vaccines are able to elicit selective immunity to a particular antigen, avoiding activation of unrelated immunity. Subunit vaccines have received great enthusiasm in attempt to develop vaccines for chronic infectious diseases such as HIV and cancer, where cytotoxic $CD8^+$ T cells responses are needed. Unfortunately, subunit vaccines are usually poorly immunogenic and require co-administration of adjuvants and/or delivery carrier to generate an effective immune response. Synthetic particulate delivery systems combined with immunological cues which mimic the natural pathogens are of particular interest in vaccine applications. In the past three decades numerous delivery systems based on nano- or micro-sized particles have been investigated preclinically and technologies have already been introduced to the clinic. Particle-based delivery systems have significant advantages over their nonformulated counterparts. For example, nanoparticles can protect antigen from degradation, co-deliver antigen and immune stimulatory signals, and enhance antigen uptake by targeting the immune system.[27-30] It has been demonstrated that the cell-mimicking approach enables cellular endocytotic pathways

to be optimized in the lysosomes entry to uptake nanoscale particles[31-34], and the resulting biomimetic nanoparticles have been used for various biomedical functions, including bioscavenger applications for toxin neutralization[35, 36] and antibacterial vaccine strategy for immunomodulation[37-40]. Previous studies also showed biomimetic nanoparticles containing both tumor-specific antigen and adjuvant generated strong antigen specific immune responses[41] and potent anti-tumor efficacy.[42, 43]

Despite intensive research, only a few of the particulate system reach clinical trials and the results are rather disappointing, especially for cancer vaccines. This highlights the needs for new system which can efficiently target vaccine components to antigen presenting cells (APCs) and elicit the desired immune responses. An important mechanism underlying the use of nanomaterials in vaccine is that of functional mimicry of natural pathogens. Nanoparticles mimic the size, charge and surface features of pathogens and preferably captured by immune cells. Here we describe a lipid-coated silica nanoparticle (SiNPs) delivery system which can efficiently accumulate in the draining lymph nodes after injection. We hypothesize that immune signal decorated SiNPs, with optimized sizes (5-100 nm diameters), are capable of targeting the draining LNs (dLNs) and mimicking the size, geometry and surface features of live viral pathogens. After subcutaneous injection, these nanoparticles can accumulate in LNs, where a large portion of immune cells reside. We show that cationic silica nanoparticles can be efficiently loaded with CpG oligonucleotide adjuvant. Subsequent lipid coating on these nanoparticles not only improves their stability, but also markedly reduces the non-specific tissue interaction after injection. Immunization with lipid-coated silica nanoparticles potentiates the *in vivo* generation of antigen-specific cytotoxic T cells and antibody response, which in turn, lead to enhanced anti-tumor efficacy. Our findings provide a simple, efficient and safe method to target molecular therapeutics to LN to modulate the immune system.

2.2. Materials and methods

2.2.1. Preparation of CpG ODN loaded SiNPs (CS) and lipid-coated SiNPs (LCS)

SiNPs were purchased from Sigma Aldrich that were initially functionalized by triethoxypropylaminosilane (density: 1.158 g/mL). Lipids were purchased from Avanti Polar Lipids except mPEG-DSPE (from Laysan Bio). The size of SiNPs was less than 30 nm and was confirmed by dynamic light scattering (DLS) measurements (Malvern Zetasizer). The SiNPs solution was diluted 10 times using D.I. water to decrease the nanoparticle density (0.116 g/mL) and added to desired amount of CpG to prepare CpG-loaded SiNPs with different weight ratios (SiNPs/CpG) such as 10, 30, 60, 90, and 150. The probe-sonication was performed for 1 min with 2/2s on/off working cycle at a power output of 4 joules. During encapsulation, CpG was fixed onto positively charged SiNPs and was subsequently coated with lipid. To coat the SiNPs with lipid bilayer, a mixed lipids (cholesterol/DOPC/DSPE/mPEG-DSPE at molar ratio of 31.5:45:13.5:10) were used. Lipids mixture were first suspended in chloroform and the solvent was evaporated to form a lipid film. These films were then placed in a chemical hood connected to a vacuum chamber over night to remove trace amounts of organic solvent impurities. Following the addition of the 1 mL of particle suspension to the coated lipid film, probe-sonication was performed for 20 min with 15/15s on/off working cycle at a power output of 4 joules. Since the suspension contained coated particles and can be separated by centrifugation, free liposomes were removed by centrifugation at 15,000 rpm for 10 min, followed by washing three times in saline.

2.2.2. Size and zeta potential measurements

To measure the size and zeta potential of nanoparticles, Dynamic light scattering (DLS, Zetasizer, Malvern) was used with He-Ne laser (633 nm) at 90° collecting optics at 25 °C. The measurements were performed with the nanoparticles suspended in saline. The surface morphology and microstructures were analyzed using a high-resolution transmission electron microscopy (HR-TEM, JEOL 2010). For TEM analysis, microfilms were made by placing a drop of the respective nanoparticle suspensions onto a 200 mesh copper TEM grid (Ted Pella, CA) and then dried at room temperature for 3 h. To visualize the lipid bilayer on nanoparticles, 2 % phosphotungstic acid (1:1 v/v) was used for negative staining. A minimum of four images for each sample was captured, and representative images were included in Figure 2-7.

2.2.3. In vitro characterization

HEK-Blue™-mTLR9 cells were purchased from InvivoGen and were used to evaluate adjuvant activity in vitro. The cells were cultured in RPMI (Thermo Fisher), containing 10 % FBS, 100 U/ml penicillin, 100 μg/ml streptomycin, and 2mM L-glutamine. Inducible SEAP (Secreted Embryonic Alkaline Phosphatase) level were detected by HEK-Blue™ detection kit from Invivogen. Mice TLR9 (mTLR9) cells were cultured in an incubator at 37 °C and then were transferred into a 96-well plate. Nanoparticles or soluble CpG were added to per well of 96-well plate and after 24 h incubation, the stimulation of mTLR9 cells was assessed by measuring the levels of SEAP secretion using QUANTI-Blue^{TM} quantitatively measured by a spectrophotometer at 645 nm.

2.2.4. Analysis of cellular uptake

DC 2.4 cells were kindly provided by Dr. Wei (Barbara Ann Karmanos Cancer Institute, Detroit, MI). To determine the intracellular delivery capacity of nanoparticles, the DC2.4 cells were seeded on glass coverslips in 6-well microscopy chamber at a density of 2 x 10^4 cells per well for 24 h at 37 °C. After 24 h, cells were treated with 10 μg/ml of fluorescence labeled CpG in soluble or in nanoparticle form for 2 h, and then washed with saline. For fixation, the glass that cells adhered on was immersed in 4 % paraformaldehyde in saline for 10 min at room temperature. Following fixation, the glass was washed with saline and mounted on a slide with nuclei staining by DAPI. Fluorescence images were obtained using a confocal microscope (Zeiss LSM 510) with a filter set of DAPI and FITC excitation/emission. For the FACS analysis, DC2.4 cells were seeded on 6-well plates at a density of 4.5 x 10^5 cells/well in the culture medium. Fluorescently labelled CpG in soluble or in nanoparticle form were added to each well and incubated for 0.5 h, 1h, and 2 h, respectively. After washing with saline, the cells were analyzed using a flow cytometer (Attune Focus). A minimum of 100 events were collected.

2.2.5. *In vivo* lymph node targeting

All animal studies were approved by the division of laboratory animal resources (DLAR) and animals were cared in the DLAR animal facility under federal, state, local, and NIH guidelines for animal care. Groups of C57BL/6 (n=2) were injected subcutaneously with 3 nmol of fluorescein-labelled CpG in soluble or in nanoparticle formulations. After 24 h or 30 h, LNs were digested with 1.5 mL of freshly prepared enzyme mix comprised of RPMI-1640 containing 0.8 mg/mL Collagenase/Dispase (Roche Diagnostics) and 0.1 mg/mL DNase (Roche Diagnostics) and LN cells were stained with antibodies against F4/80 and CD11c

versus CpG fluorescence in viable cells. Percentages of CpG^+ cells in the LNs were determined by flow cytometry at 24 h or 30 h.

2.2.6. Immunization

Groups of C57BL/6 mice (n=3 per group) were immunized by subcutaneous injection on day 0 and day 14 with 10 μg ovalbumin (OVA) or 10 μg DSPE-PEG-OVA-II (amph-OVA-II) plus CpG in soluble or in nanoparticle based adjuvants. Seven day after the final immunization (day 21), mice were bled and peripheral blood mononuclear cells were evaluated by SIINFEKL/H-$2K^b$ peptide-MHC tetramers staining and intracellular cytokine (IFN-gamma and TNF alpha) staining. To assess the functionality of primed $CD8^+$ T cells, peripheral blood mononuclear cells were stimulated *ex vivo* with 10 μg/mL OVA peptide SIINFEKL for 6 h with Brefeldin-A, fixed, permeabilized, stained with anti-IFN-γ, anti-TNF-α, and anti-CD8α, and analyzed by flow cytometry. Anti-OVA IgG titers, defined as the dilution of serum at which 450 nm OD were determined by an enzyme-linked immunosorbent assay (ELISA) analysis. To determine antibody titers, ELISA plates (eBioscience) were coated with 10 μg/mL of OVA in saline overnight at room temperature. The plates were blocked with 200 μL of 1% bovine serum albumin (BSA) in saline for 1 h. Serum was serially diluted in saline between $1:10^2$ and $1:10^7$, and applied to the plate and incubated for 1 h at room temperature. Peroxidase-conjugated goat anti-mouse IgG (HþL) (1:5000 in 1% BSA-PBST, 100 μL/well) was then applied for 1 h, and the plates were developed using TMB substrate (100 μL/well, eBioscience). The reaction was stopped using 50 μL of 1 M sulfuric acid and absorbance values were measured at 450 nm. Interlukin (IL)-6 and IL12 were also analyzed using cytokine-specific ELISA (BD Biosciences) according to the manufacturer's instructions.

2.2.7. Tumor model

EG.7-OVA cells (Mouse thymoma EL4 cells) were purchased from ATCC and 2 x 10^6 cells were subcutaneously inoculated into the right flank of 5-6-week-old C57BL/6 mice. When the tumor mass became palpable (7-8 mm, typically 5 days later), mice were divided into five treatment groups (n=6) and the tumor-bearing mice were subcutaneously injected with 20 μg OVA or 20 μg amph-OVA-II plus 1.24 nmol CpG in nanoparticle form. Survival and tumor size were measured everyday using a sliding caliper. The tumor volume was calculated using the following formula: tumor volume (mm^3) = length x $(width)^2/2$.[44]

2.2.8. Statistical analysis

To analyze the statistical difference between groups, a one-way analysis of variance (ANOVA) with Tukey's HSD post-hoc test was used. All of the values are expressed as means ± standard deviations. GraphPad Prism software was used for all the statistical analyses. ****P<0.0001, ***P<0.001, **P<0.01, *P<0.05. NS, not significant.

2.3. Results and discussion

2.3.1. Design of LN-targeting CpG loaded SiNPs

A major obstacle in subunit vaccines is the insufficient delivery of the vaccine components to the lymph nodes. Vaccine delivery by nanocarriers could make a big impact on the treatment of infectious diseases as well as on cancer immunotherapy. Properties of nano-sized vaccine carrier are highly tunable. For example, surface of nanocarriers can be easily modified to expose either antigen or adjuvant (or both), allowing co-delivery of antigen and immune signal to LNs, which result in greater lymphocyte priming. In this respect, porous

nanoparticles such as mesoporous SiNPs[45] or nanoporous polymer-based spheres[46] have been employed with some success for vaccine delivery. However, extra steps are needed to fabricate the templates, which involve complex chemical and physical process occurring at several times. It is also costly for the fabrication of large-scale mesoporous SiNPs with controlled pore orientations.[47-49] In addition, the vaccine encapsulation efficiency and the bioaccessibility of loaded vaccine also need to be addressed in more detail.[45] Although drug delivery systems via nanoparticles[50-54] has been gaining momentum in the past decade, the development of simple and efficient delivery vehicles for *in vivo* applications, especially for delivery to LNs, has remained a major challenge.

To prepare the pathogen mimicking SiNPs with stimulatory DNA encapsulated, we choose a cationic silica nanoparticle. Cationic nanoparticles have been widely used to condense DNA in transfection. Briefly, amine modified SiNPs (30 nm) were complexed with CpG DNA, a single-stranded synthetic oligodeoxynucleotides with cytosine-phosphate-guanine motifs that can activate the APCs expressing the pathogen recognition receptor Toll-like receptor 9 (TLR9). We first prepared fluorescein amidite (FAM)-labelled CpG-loaded SiNPs (CS) with different weight ratios (SiNPs/CpG) of 10, 30, 60, 90, and 150 to find the optimum loading ratio of CpG DNA on SiNPs, focusing on the nanoparticle's stability (Figure 2-1a and b). The desired amount of SiNPs were simply added to fluorescence labelled CpG solution and briefly probe-sonicated, following 1 h incubation at room temperature (figure 2-1c). 10, 30, 60, and 90 ratio CS showed a precipitated layer on the bottom of 1.5 mL microcentrifuge tubes, emitting green fluorescence under the UV lamp, implying that the interaction between SiNPs and CpG DNA was sufficient to promote significant aggregation of nanoparticles (defined here as formation of clusters of three or more nanoparticles). In contrast, soluble 3'-FAM CpG DNA and 150 ratio CS showed uniform green fluorescence, indicating a formation of stabilized NPs.To further confirm their soluble stability, brief

centrifugation (5,000 rpm for 5 s) was performed for all samples and 150 ratio CS showed excellent solution stability (no precipitate layer) that was similar to soluble 3'-FAM CpG DNA (Figure 2-1d). To quantify the amount of CpG DNA absorbed onto the SiNPs surface, the supernatant after centrifugation was analyzed by UV-vis measurement (Figure 2-1e). The amount of CpG DNA in the supernatant decreased with increasing the SiNPs/CpG weight ratio from 10 up to 60, but it was increased when the surface coverage of CpG DNA on SiNPs was reduced (90 and 150 ratio CS). Those two 90 and 150 ratio CS showed a characteristic DNA adsorption curves under the UV region, which also were slightly lifted up compared to other curves, indicating detected CpG DNA from 90 and 150 ratio CS were originated from the surface of SiNPs, not from soluble CpG DNA. In particular, 150 ratio CS showed the equivalently same level of peak intensity measured from soluble CpG DNA, indicating 150 ratio CS was uniformly distributed in the solution. The saturation point was found at 60 ratio CS, representing the loss of CpG DNA from SiNPs was less than 5 %. At this ratio, SiNPs were expected to be fully covered by CpG DNA, enabling high loading of CpG DNA per nanoparticle, but 150 ratio CS looked more reasonable for vaccine delivery in terms of their colloidal stability. The 150 ratio CS was relatively stable in serum, releasing 20 % of the adsorbed CpG DNA when incubated in the presence of 10 % serum at 37 ^{o}C for 3 days (Figure 2-1g).

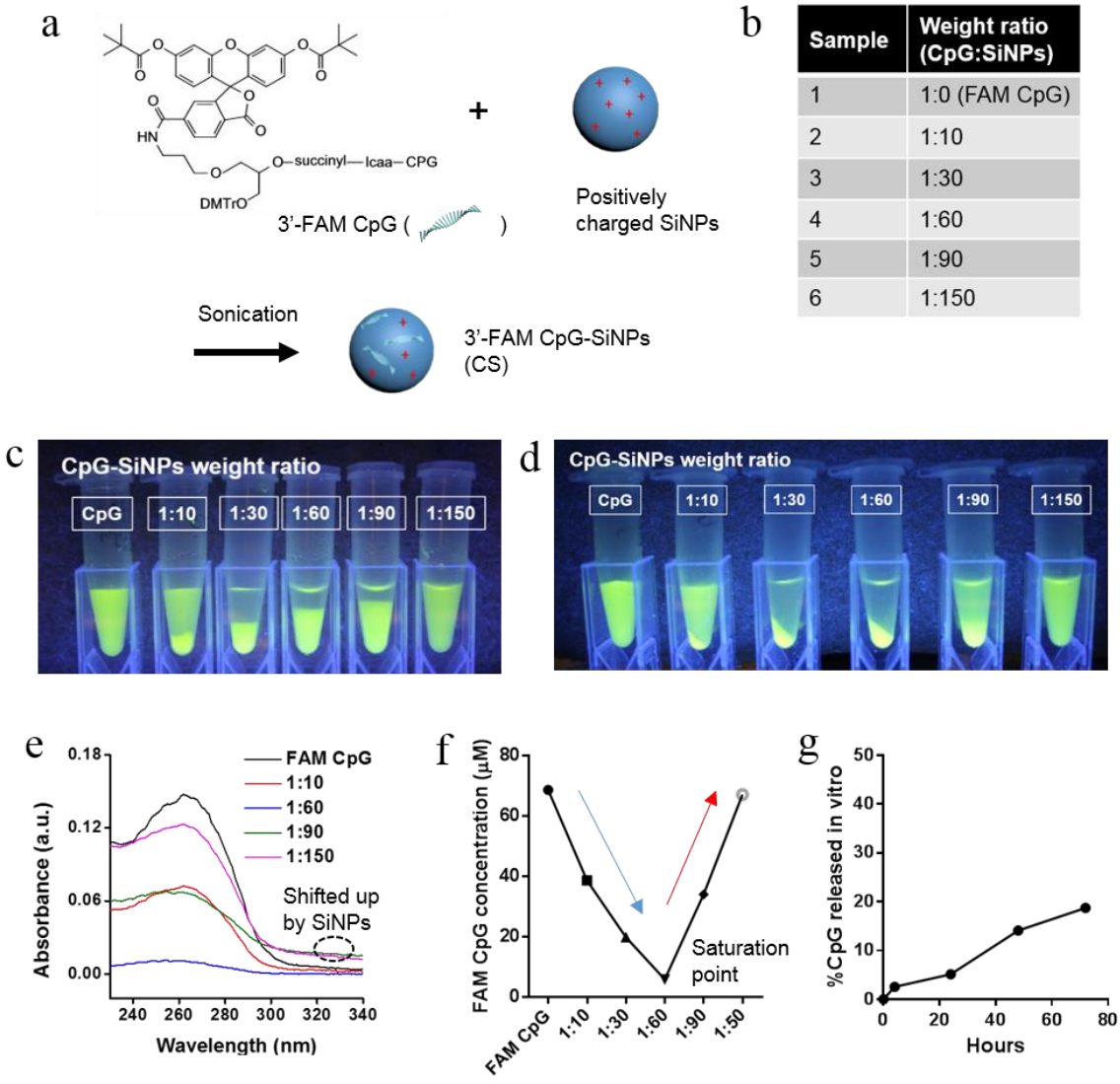

Sample	Weight ratio (CpG:SiNPs)
1	1:0 (FAM CpG)
2	1:10
3	1:30
4	1:60
5	1:90
6	1:150

Figure 2-1. a) Illustration of FAM CpG-SiNPs preparation based on their charge interactions. b) Table showing CS with their different weight ratios in the study. c) Fluorescent image showing CS samples after incubation at room temperature for 1 h. d) Image showing CS samples after brief centrifugation (5000 rpm for 5 second). e) UV-vis absorbance from the supernatant of CS samples. f) FAM CpG concentration measured from the supernatant of CS samples. g) Kinetics of FAM CpG DNA release from nanoparticles incubated in saline containing 10 % serum at 37 ºC.

Motivated by above findings, the aggregation of nanoparticles was ascertained by DLS measurements. In view of the results shown in Figure 2-2a, the size of CS decreased with increasing SiNPs/CpG DNA weight ratio, indicating their aggregation was more significant when SiNPs were fully covered by CpG DNA. Only 150 ratio CS showed monodisperse in size (45 nm) and uniform in loading, two features of utmost importance for reliable adjuvant dosage. The results from zeta-potential measurements showed a positively charged surface feature from bare SiNPs, which reflects strong electrostatic interactions with negatively charged CpG ODN (Figure 2-2b). The surface saturation point shown in Figure 2-1f was corroborated by zeta-potential measurements, which showed a progressive decrease in surface potential from 31 mV for SiNPs to 4 mV for the 60 ratio CS. Since the 10, 30, 60, and 90 ratio CS gave very large aggregates, the 150 ratio CS was selected for further vaccine studies. The potential profiles in the stern layer and the diffusion layer are illustrated in Figure 2c based on potential in SiNPs. The 150 ratio CS covered partially by CpG DNA has positively charged surface (~15 mV) and creates an electrostatic field that affects the ions in the bulk of the liquid, thereby creating an electric double layer. Thus it can be said that particles tend to segregate into a layer adjacent to the layer of surface charges in SiNPs, showing better colloidal stability of nanoparticles.

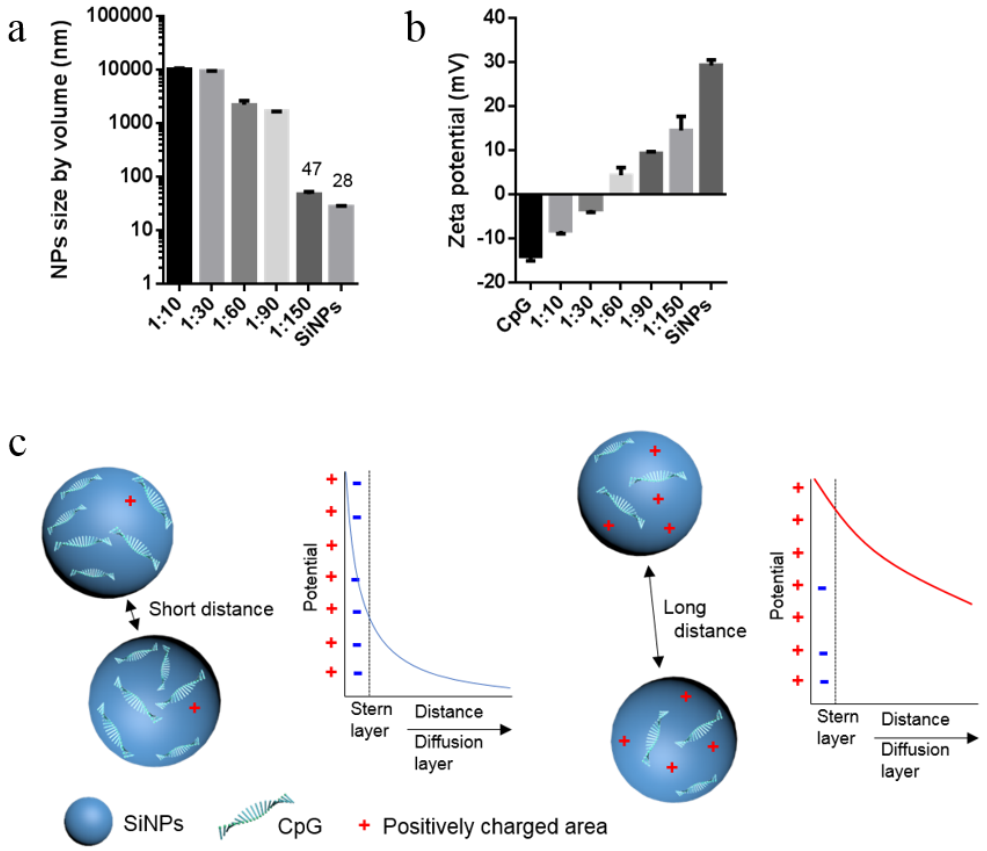

Figure 2-2. a) NPs size by volume. b) NPs zeta potential. c) Expected distance between two CS particles with low and high weight ratio, and its expected distance of diffusion layer.

2.3.2. SiNPs formulation efficiently targets CpG to the LN.

It is well known that the parenteral administration of unformulated CpG DNA fails to reach lymph nodes (LNs), the anatomic organ where the primary function of immune cells is orchestrated. Thus, efficient LN-targeting strategy has the key roles in promoting immune activation and has the great potential to transform disease treatment. To see whether 150 ratio CS reflect sufficient transport of CpG DNA to dLNs, we assessed LN accumulation following subcutaneous injection, using a fluorophore-conjugated derivative to enable detection of CpG in the tissue (Figure 2-3a). The CS with different weight ratios were injected in

C57BL/6 mice (n = 2 per group), and 24 h later, dLNs were excised (Figure 2-3b). The LNs from mice injected with 60, 90, and 150 ratio CS showed bigger inguinal or axillary LNs than LNs from mice injected with soluble CpG DNA or saline (Figure 2-3c). On the other hand, mice injected with 180 ratio CS showed swelling at the injection site and it last one week from the day of administration (Figure 2-3d). By injecting 300 ratio CS into mice, inflammation occurred in response to redness and tissue damage. Strongly cationic particles are known to be toxic and to interact more favorably with the tissue thereby inducing inflammation.[55, 56] However, in contrast to the results above, mice injected with 150 ratio CS showed a semblance of normality. By flow cytometry, 30, 60, and 180 ratio CS exhibited low accumulation in $CD11c^+$ DCs or $F4/80^+$ macrophage, whereas 150 ratio SiNPs showed marginally increased uptake in inguinal or axillary LNs (Figure 2-3e, f, and g). This results implies that 150 ratio CS has a reasonable fit of surface charge that can enhance delivery of CpG DNA to lymphatics and promote their capture in dLNs without any inflammations at the injection site. Inefficient capture of CpG DNA in LNs is consistent with the low molecular weight of soluble CpG DNA, big size of lower weight ratio CS, and swelling or tissue damage from the injection of 180 ratio CS, which will be capable of absorption directly into blood capillaries at the injection site.

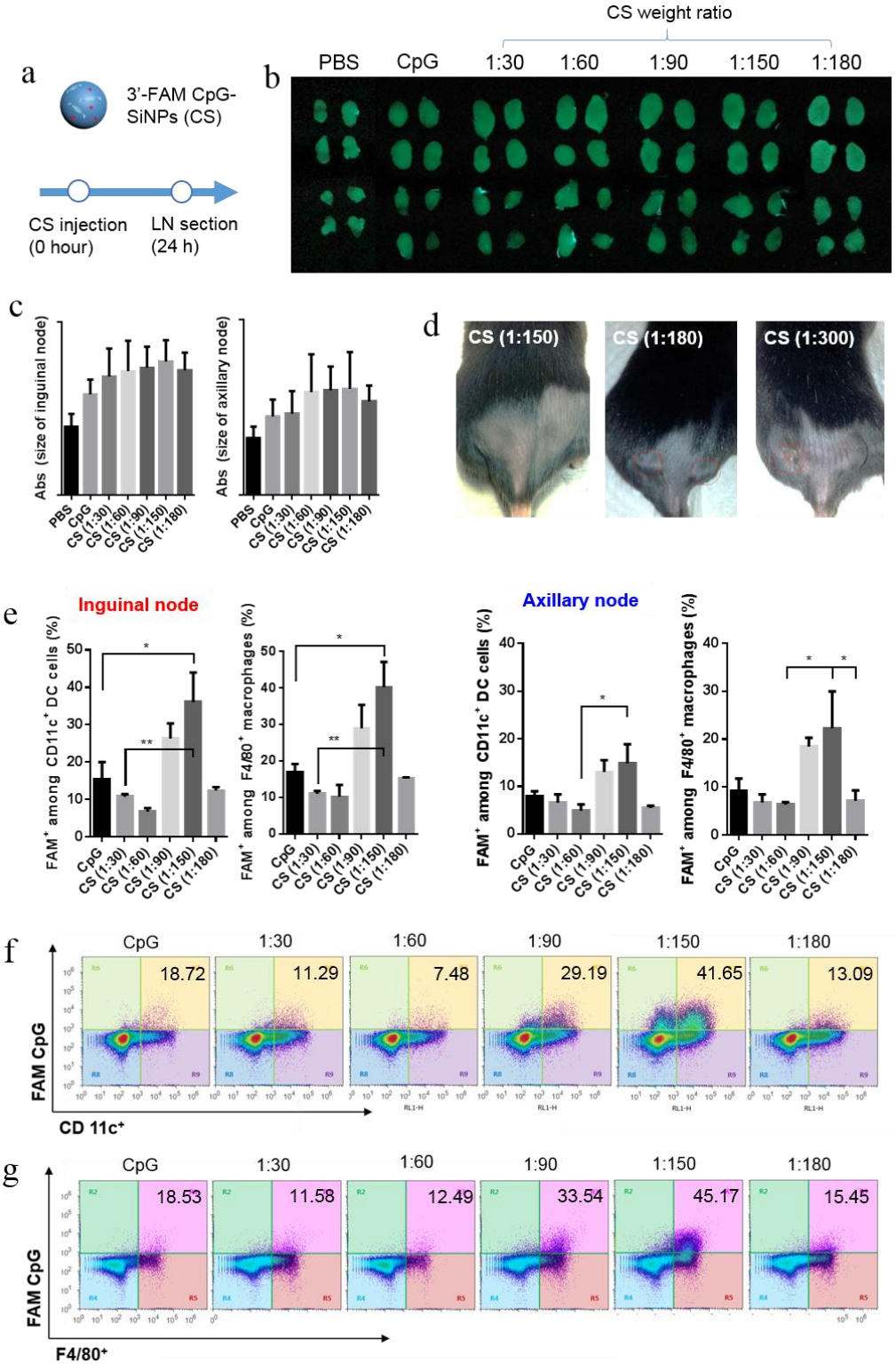

Figure 2-3. a) Quantification of CpG DNA in LNs after injection of fluorescent-labeled CpG DNA in soluble or nanoparticle form. b) image showing excised draining LNs from C57BL/6 mice (n=2 LNs per group) injected with fluorescent-labeled CpG DNA (3 nmol) in soluble

or in nanoparticle form. c) size of inguinal and axillary lymph nodes measured by image J. d) image showing injection sites of 150, 180, and 300 ratio CS measured two weeks after injection. e) CpG^+ cells determined by flow cytometry at 24 h compared with soluble CpG DNA. f) representative flow cytometry plots of F4/80 staining and g) CD11c staining.

Given the enhanced delivery of CpG DNA by 150 ratio CS, we examined LN accumulation again after 30 h using same SiNPs. We questioned ourselves that they may have nonspecific interaction with serum protein/matrix because of their positively charged surface, and hence the rate of uptake may slow, compared to negatively charged free CpG DNA. The 150 ratio SiNPs were injected in C57BL/6 mice, and 30 h later, dLNs were excised (Figure 2-4a). Nanoparticles showed 1.6-fold greater accumulation in $CD11c^+$ DCs and also in $F4/80^+$ macrophage in inguinal node (Figure 2-4b, c, and d). This results implies that 150 ratio CS may move slower than negatively charged CpG ODN to reach dLNs. Further studies are under investigation whether their slower kinetic is beneficial for vaccine delivery.

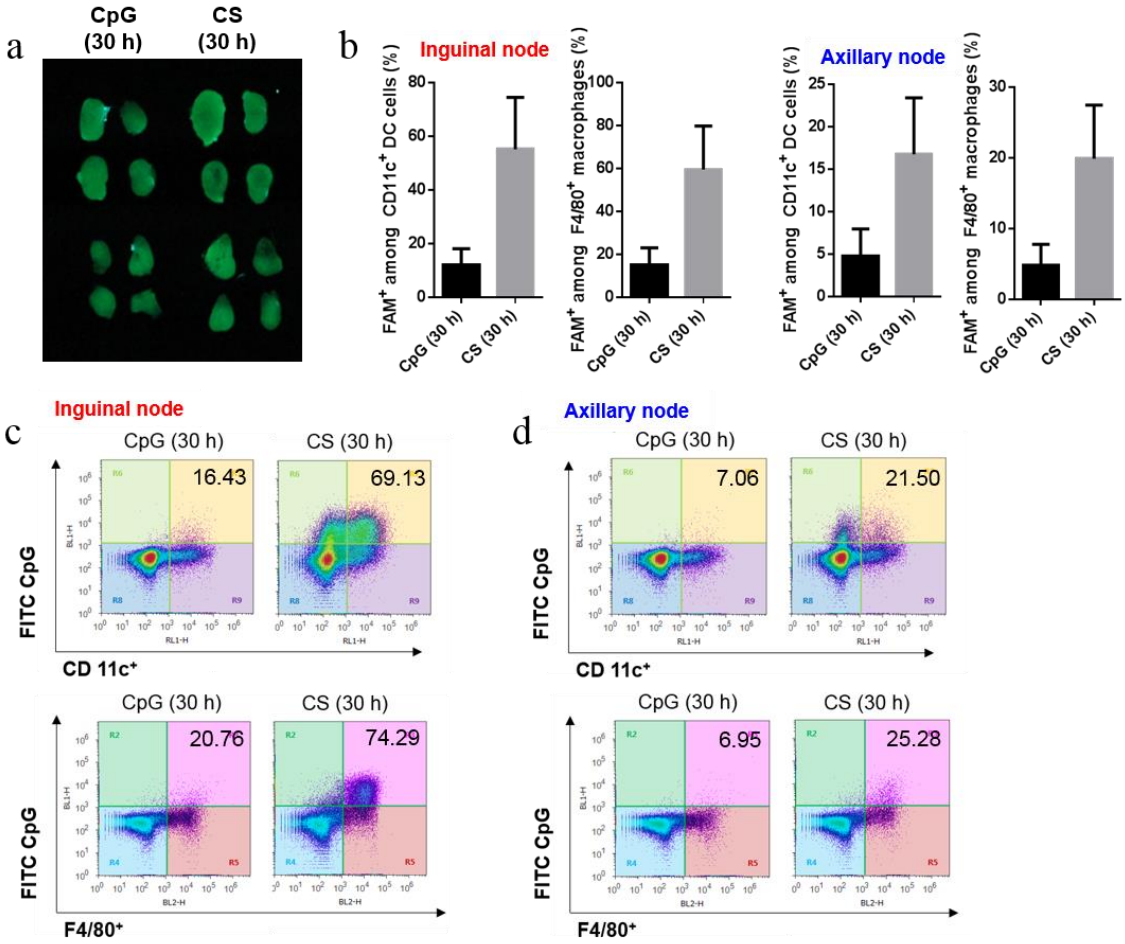

Figure 2-4. a) Imaging of excised draining LNs at 30 h from C57BL/6 mice (n=2 LNs per group) injected with fluorescent-labeled CpG (3 nmol) in soluble or nanoparticle form. b) CpG^+ cells determined by flow cytometry at 24 h. Representative flow cytometry plots of F4/80 staining and CD11c staining from c) Inguinal node and d) Axillary node.

2.3.3. Design of LN-targeting lipid coated SiNPs and pathogen mimicking composite materials.

It is well known that PEGylated lipid nanoparticles that can mimic the natural pathogens enable better retention of encapsulated drugs, and modestly enhance their lymphatic uptake.[57] To prepare lipid coated SiNPs, we used a coated lipid film method[49] in which nanoparticles

were added to a continuous lipid film coated onto a round-bottom small tube surface, allowing uniform coating. This method leads to complete nanoparticle coating, providing effective vaccine sealing without the necessity to conduct an extrusion or multiple washing procedures. For LCS fabrication (Figure 2-5a), The 31.5:45:13.5:10 molar ratio of cholesterol/DOPC/DSPE/mPEG-DSPE in chloroform was dried under nitrogen followed by incubation under vacuum at room temperature overnight. The resulting lipid films were resuspended to a concentration of 0.116 g/ml nanoparticles and probe-sonicated for 20 min with 15/15s on/off working cycle. It has been demonstrated that cholesterol can enhance transfection efficiency in liposome-based formulations, and PEGylated lipid reduces nonspecific interactions of vesicles with serum proteins/matrix, enabling better retention of encapsulated vaccine.[58-60] Importantly, the majority of the lipids were found to coat the SiNPs instead of forming empty liposomes, as rhodamine labeled lipid settled along with the SiNPs on the bottom of the tube after brief centrifugation (Figure 2-5c). In contrast, sample prepared without CS showed no sediment layer after centrifugation (Figure 2-5b). We suspected the positive amines on the surface of SiNPs might interact with lipids and initiate the lipid bilayer formation.

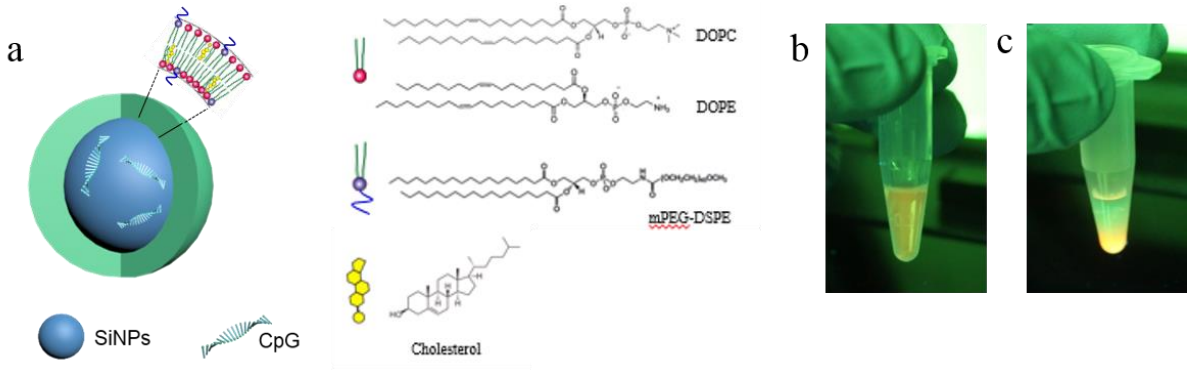

Figure 2-5. a) Schematic diagram of LCS and structure of DOPC, DOPE, mPEG-DSPE, and Cholesterol. b) Image showing rhodamine-conjugated lipid and c) rhodamine-conjugated lipid with nanoparticles dissolved in saline after centrifugation (21 G for 10 min), the majority of the lipids settled along with CS nanoparticles.

The surface of LCS was further functionalized with OVA-II peptide that can efficiently delivery OVA-II antigen and adjuvant to APCs at the same time. An ideal vaccine is one that is able to mimic the immunological response by a naturally occurring infection. This surface functionalization makes nanoparticles more "pathogen-mimicking" in respect to their intracellular fate, persistence and APC activation compared to Yersinia pestis or Escherichia coli.[61] The amphiphilic antigen was anchored on the lipid-coated SiNPs using a post insertion method.[62] We first prepared amph-OVA-II (Figure 2-6a) using a method described previously[63] and added it into LCS solution to prepare OVA-II functionalized LCS (Figure 2-6b). In short, Maleimide-PEG_{2000}-DSPE and OVA-II peptide were dissolved in Dimethylformamide (DMF) separately, and they were mixed and agitated at room temperature for 24 hours, following the addition of Triethylamine (TEA) for their coupling (Figure 2-6a). The prepared amph-OVA-II was added to LCS solution and probe-sonicated for 1 min with 2/2s on/off working cycle. This nanoparticle will be demonstrated as a

multifunctional carrier for co-delivery of both OVA-II antigen and CpG ODN adjuvant to APCs in stimulating antigen-specific $CD4^+$ T cell responses.

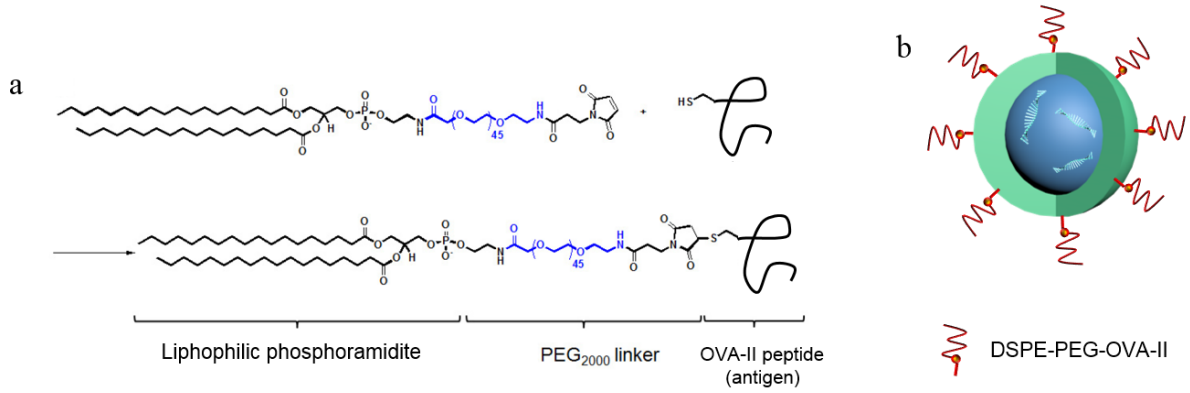

Figure 2-6. a) OVA-II peptide with amino-terminal cysteines were conjugated to maleimide-PEG_{2000}-DSPE. b) OVA-II functionalized LCS (LCS composite combined with amph-OVA-II)**.**

The surface morphology and microstructures of nanoparticles were analyzed using HR-TEM. To visualize the lipid bilayer, 2 % phosphotungstic acid (1:1 v/v) was used for negative staining. Figure 2-7a showed SiNPs with an overall spherical shape and some surface roughness (black dots). The image of SiNPs without staining showed its smooth surface (no black dots), implying that black dots were originated from aminosilane functional groups on the surface of SiNPs (data not shown). The CS image showed no difference in their morphology compared to bare SiNPs (Figure 2-7b). However, the SiNPs from LCS were found to be surrounded by a continuous ring of ~ 4 nm distance which is consistent with the known thickness of a lipid bilayer.[64, 65]

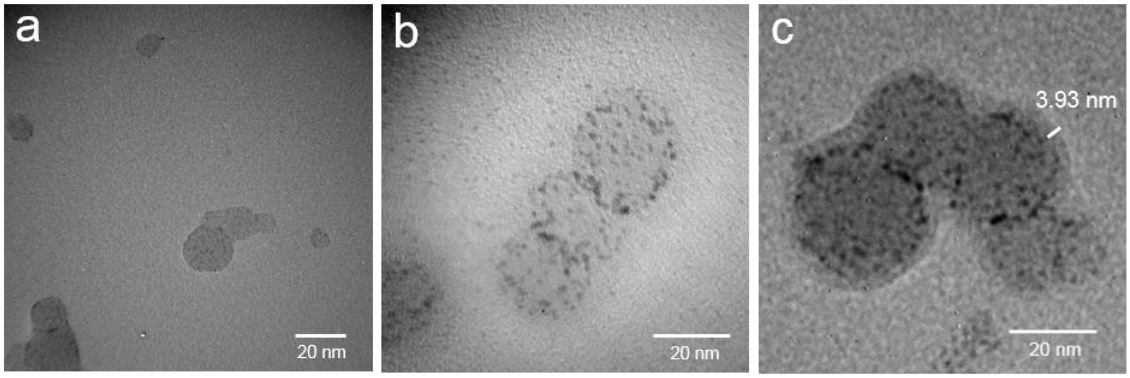

Figure 2-7. Transmission electron microscopy (TEM) images of a) SiNPs, b) CS, c) LCS.

2.3.4. Lipid coated SiNPs formulation efficiently targets CpG to the LN.

We prepared fluorescence-labeled LCS (Figure 2-8a) based on the procedure described in section 2.3.3 to measure their LN accumulation. It showed ~ 110 nm size, which is little bigger than CS and almost zero surface charge measured by DLS measurements (Figure 2-8b). The LCS loaded with fluorescently labeled CpG DNA were relatively stable in serum, releasing only 5 % of the encapsulated CpG DNA when incubated in the presence of 10 % serum at 37 ^{o}C for 3 days (Figure 2-8c). This result implies that nanoparticles were surrounded by lipid bilayer, enabling better retention of encapsulated CpG DNA. We next investigated LN accumulation of CpG DNA following subcutaneous injection using a fluorescence-labeled LCS. Mice treated with LCS showed bigger LNs (Figure 2-8d) and enhanced lymphatic uptakes compared to results measured by CS administration (Figure 2-8e). In addition, CpG DNA delivered via LCS platform was detected in approximately 40 % (2-fold higher than CS) of LN macrophages and DCs from axillary node.

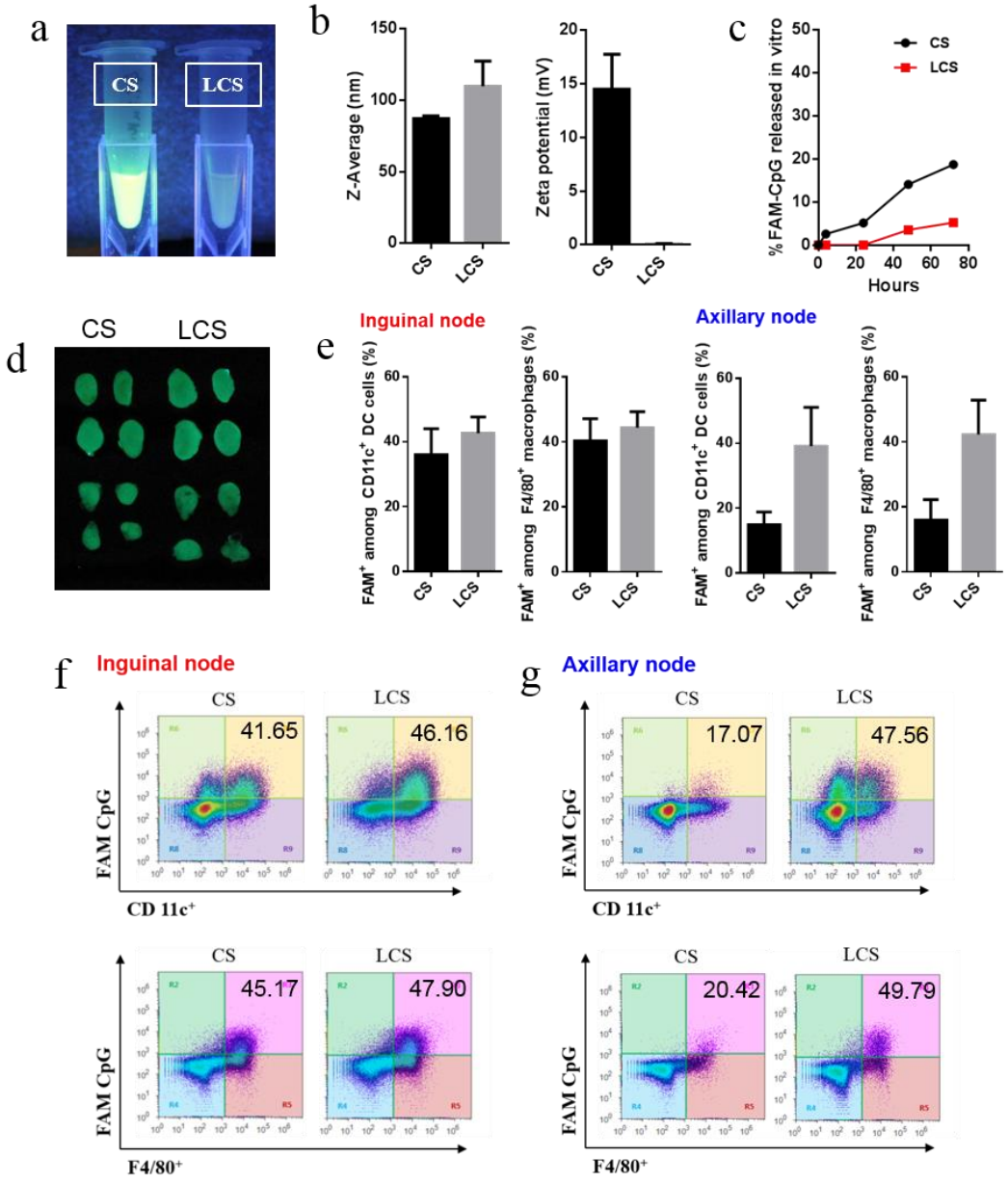

Figure 2-8. a) Fluorescent images of CS and LCS samples. b) Z-Average and zeta potentials of CS and LCS measured by DLS c) excised LNs image from C57BL/6 mice (n=2 LNs per group) injected with CS and LCS. d) size of inguinal and axillary lymph nodes measured by image J. e) CpG^{+} cells determined by flow cytometry at 24 h. Representative flow cytometry plots from cells stained withCD11c and F4/80 f) in inguinal node and g) in axillary node.

Figure 2-9 showed immunofluorescent images of inguinal LN section. Mice were injected subcutaneously with 3 nmol of fluorescein-labelled CpG DNA, CS, or LCS. After 24 h, LNs were sliced by a cryostat and LN cells were stained with antibodies against B220 and CD3. Histological sections of dLNs showed little detectable CpG DNA, whereas CS and LCS represented marginally increased CpG DNA accumulation in the subcapsular sinus and interfollicular areas.

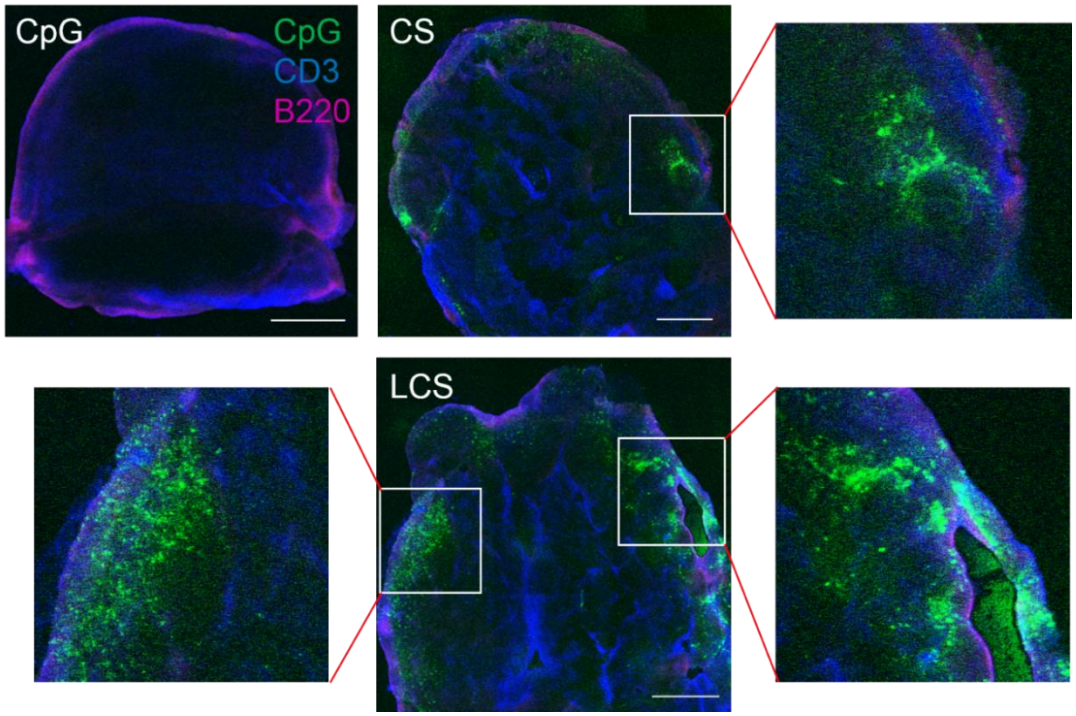

Figure 2-9. Immunohistochemistry of inguinal LNs 24 h after injection (CD3, blue; B220, pink; CpG, green).

2.3.5. SiNPs enhances cellular uptake and immune stimulation of CpG *in vitro*.

The development of ideal vaccines depends on an efficient means of transfer of vaccine components into a cell. We next studied the effect of our nanoparticle on the transfection efficiency. For the analysis of confocal laser scanning microscopy, DC2.4 cells were first seeded on glass coverslips for 24 h at 37 °C and after 24 h, cells were treated with 10 μg/ml of fluorescence labeled CpG DNA, CS, or LCS for 2 h. Following fixation, the glass was washed with saline and mounted on a slide with nuclei staining by DAPI. Bright green fluorescence was observed for cells treated with CS and LCS when excited at 435 nm, suggesting those nanoparticles could be taken up rapidly by cells (Figure 2-10a). It was also clearly observed from confocal images that LCS were more closely translocated into the perinuclear zone. By contrast, the cells that treated with soluble CpG DNA showed only weak green fluorescence. The kinetics of CpG uptake were quantified by FACS analysis (Figure 2-10b). Consistent with confocal results, free CpG showed little uptake by DC2.4 cells, in contrast, both LCS and CS nanoparticles had markedly improved uptake, though the uptake appeared to be more rapid in LCS treated cells. This results suggest that CpG DNA in nanoparticle form allowed more efficient delivery with minimal leakage into the culture medium. The SiNPs are known to have a great affinity for the head-groups of a variety of phospholipids.[45] Therefore, the high affinity for adsorbing on cell surfaces may cause enhanced endocytosis. These observations are consistent with the results of previous studies, showing that SiNPs are attractive carriers for gene transfection to cells, because the SiNPs DNA complex has a high transfection efficiency and a low toxicity.[45, 66-70]

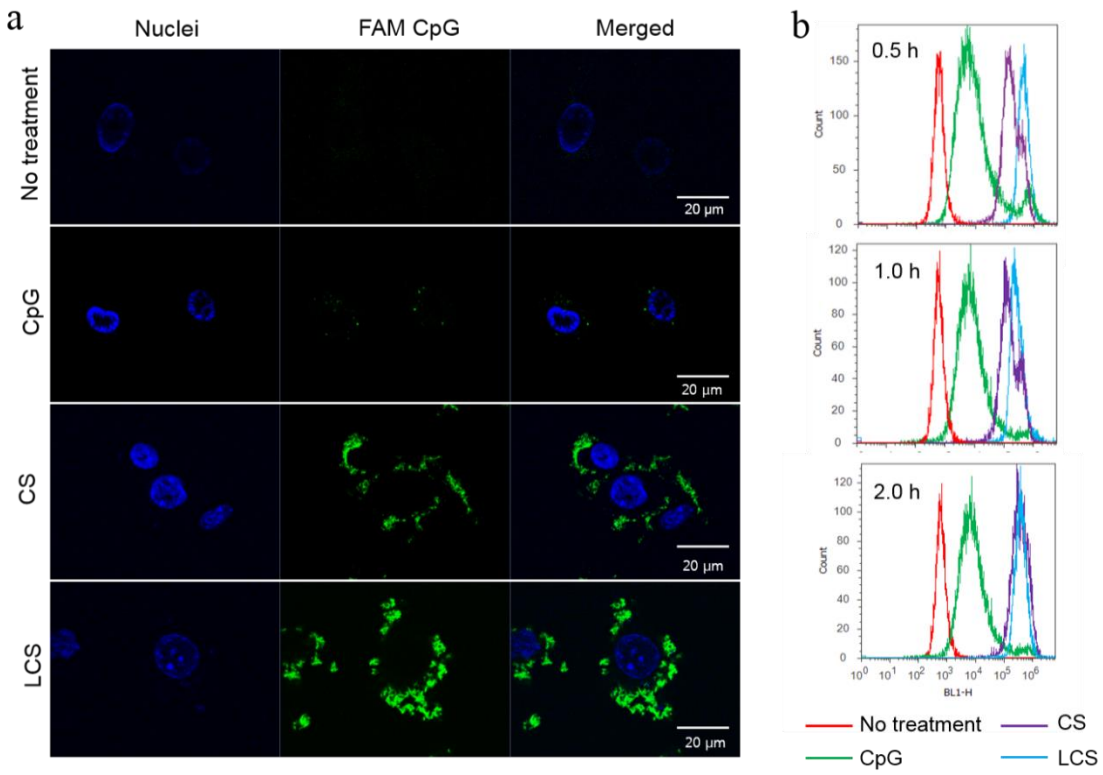

Figure 2-10. Nanoparticle delivery studied by confocal fluorescence microscopy. a) Representative confocal microscopy images of DC 2.4 cells. Cell nuclei were stained with DAPI (blue) and fluorescent-labeled CpG (green) was used to detect CpG uptake. DC 2.4 cells were incubated with adjuvants for 2 h. b) Flow cytometry assay of the uptake. DC 2.4 cells were incubated for 0.5, 1.0, or 2.0 h.

To evaluate the adjuvant activity of nanoparticles, the activation of TLR9 by different CpG formulations were measured 24 h after incubation. Both Raw-Blue and mTLR9 cells express TLR9 and are transfected with a secreted embryonic alkaline phosphatase (SEAP) reporter induced by NF-κB. Raw-Blue and mTLR9 cells were incubated with free CpG DNA, CpG with CS, or CpG with LCS at 37 ºC. After 24 hours, 20μL supernatants of cells were transferred to 200μL Quanti-Blue solution and further incubated for 1 h. The SEAP levels were determined colorimetrically at 620 nm by UV-Vis. As shown in Figure 2-11, CS and

LCS stimulated higher level of TLR receptor activation than soluble CpG DNA, which reflects nanoparticulate CpG modification do not compromise the immunostimulatory activities of CpG DNA, instead, it enhances the level of stimulation.

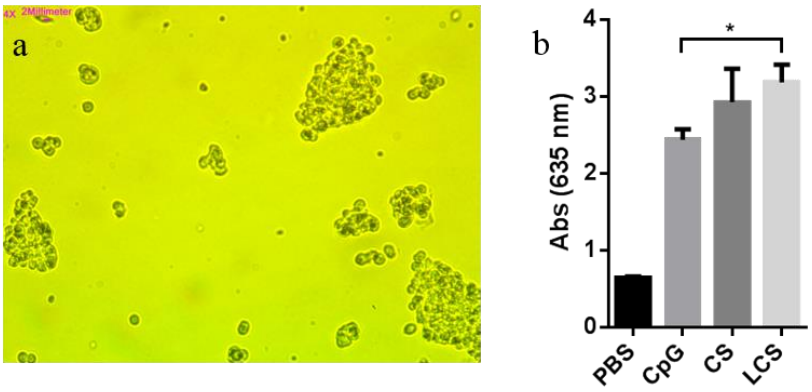

Figure 2-11. a) TLR9 cells and b) alkaline phosphatase activity in PBS, CpG DNA, CS, and LCS, measured from supernatants of cell cultures by Quanti-Blue.

2.3.6. SiNPs formulations trigger potent antigen-specific immune responses.

CpG DNA has been reported to activate cells expressing TLR9 receptor and to promote expression of costimulatory molecules from APCs that can activate T cell responses.[24, 71] To first measure the impact of nanoparticle delivery on T cell priming, C57BL/6 mice were immunized subcutaneously on day 0 and day 14 with ovalbumin (OVA) protein alone or adjuvanted by 1.24 nmol CpG DNA in soluble or in nanoparticle form. The cellular immunity was monitored by measuring OVA-specific $CD8^+$ T cell proliferation in peripheral blood using SIINFEKL/H-2Kb peptide-MHC tetramers. As expected, soluble CpG DNA induced relatively weak antigen-specific $CD8^+$ T cell responses, showing less than 4% OVA-specific $CD8^+$ T cells in blood. In contrast, LCS elicited 8-fold higher $CD8^+$ T cell proliferation

(Figure 2-12a and b). Intracellular cytokine staining was also carried out at 7 days after boost on peripheral blood mononuclear cells restimulated with SIINFEKL peptide to identify cytokine-producing antigen-specific T cells. LCS-adjuvanted vaccines induced 3-fold and 3.5-fold greater total cytokine$^+$ production in $CD8^+$ and $CD4^+$ T cells, respectively, compared with vaccination by soluble CpG DNA adjuvant (Figure 2-12a). These results imply that nanoparticle delivery generate a higher frequency of $CD8^+$ T cells producing both IFN-γ and TNF-α, which are critical for innate and adaptive immunity against intracellular antigens.[72] We further assessed IL-6 and IL-12 production in the sera of immunized mice. Nanoparticle delivery induced higher IL-6 and IL-12 production compared to vaccination with soluble CpG DNA (Figure 2-12c). IL-6 has been reported to be involved in the generation of Th2 immune response.[73] In contrast, IL-12 production involves multiple signaling pathways in the production of IFN-γ and TNF-α from T cells and natural killer (NK) cells.[22] They mediate enhancement of the cytotoxic activity of NK cells and $CD8^+$ cytotoxic T lymphocytes.[74] Our result suggests that CpG DNA in nanoparticle form induce a potent immune response through cell-signaling pathway including MyD88-dependent nuclear factor-κB (NK- κB)[75] and mitogen-activated protein kinase (MAPK)[76] pathways, which can induce the secretion of proinflammatory cytokines such as TNF-α, IL-6, and IL-12.[15]

Additionally, we evaluated the functional capacity of amphiphilic OVA-II peptide functionalized LCS elicited T cell response through detection of IFN-γ production following re-stimulation of peripheral blood mononuclear cells on day 21 with OVA-II peptide (Figure 2-12d and e). The results showed enhanced cytokine production by $CD4^+$ T cell induced by OVA-II functionalized LCS adjuvanted administration for specific antigen dependent production of IFN-γ.

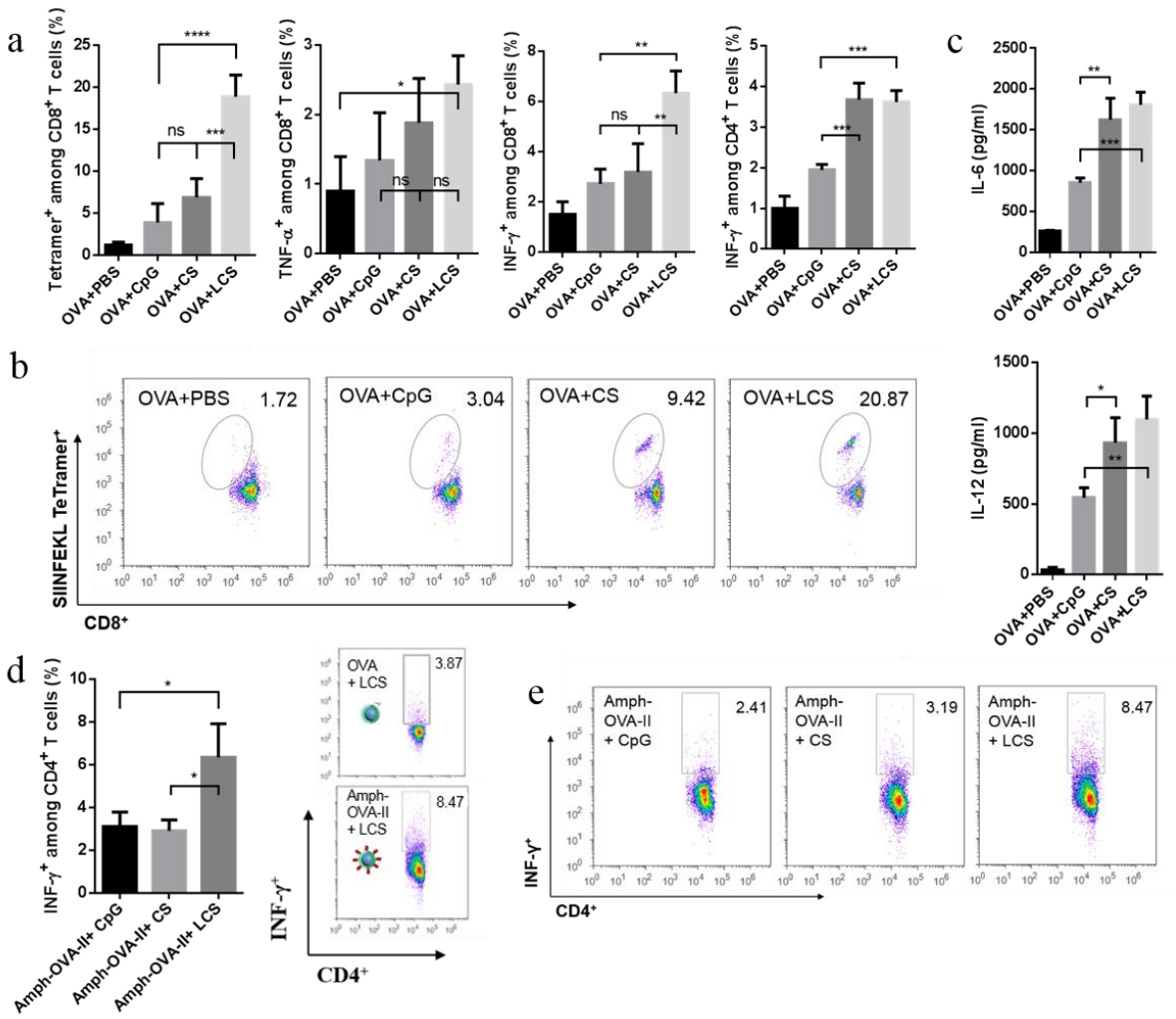

Figure 2-12. Groups of C57BL/6 mice (n=3 per group) were immunized subcutaneously on day 0 and day 14 with 10 μg OVA and 1.24 nmol CpG DNA, CS, or LCS formulations. PBMCs were restimulated ex vivo with $CD8^+$ and $CD4^+$ OVA epitopes and analyzed by flow cytometry for intracellular cytokine staining. a) Mean percentages of OVA specific $CD8^+$ T cell and TNF-α^+ or IFN-γ^+ T cell frequencies. b) Representative flow cytometry plots of OVA-specific $CD8^+$ T cells. c) Levels of IL-6 and IL-12 productions in mice sera detected 3 weeks after immunization. de) IFN-γ^+ $CD4^+$ T cell frequencies from each group of C57BL/6 mice (n=3 per group) immunized subcutaneously on day 0 and day 14 with 10 μg Amph-OVA-II and 1.24 nmol CpG DNA, CS, or LCS formulations.

We measured the level of OVA-specific IgG in the sera of immunized mice to compare the capacity for generating humoral immunity. Measurement of the IgG level gives insight into the types of T helper cell immune responses. It is well known that the immune system responds to CpG motifs by activating potent Th1-like immune responses.[21] To evaluate the antibody response elicited by soluble CpG DNA or CpG DNA in nanoparticle form, sera from immunized mice were collected on day 21 following a prime on day 0 and boost on day 14. ELISA measurements of serum titers of OVA-specific IgG showed higher levels of anti-OVA IgG in mice immunized by nanoparticle formulations (Figure 2-13a). Mice immunized by OVA-II functionalized nanoparticles showed significant increases in serum titers against anti-OVA-II IgG (Figure 2-13b). These nanoparticle-mediated CpG DNA with antigen delivery enable robust humoral immune responses with higher levels of antigen-specific antibody productions.

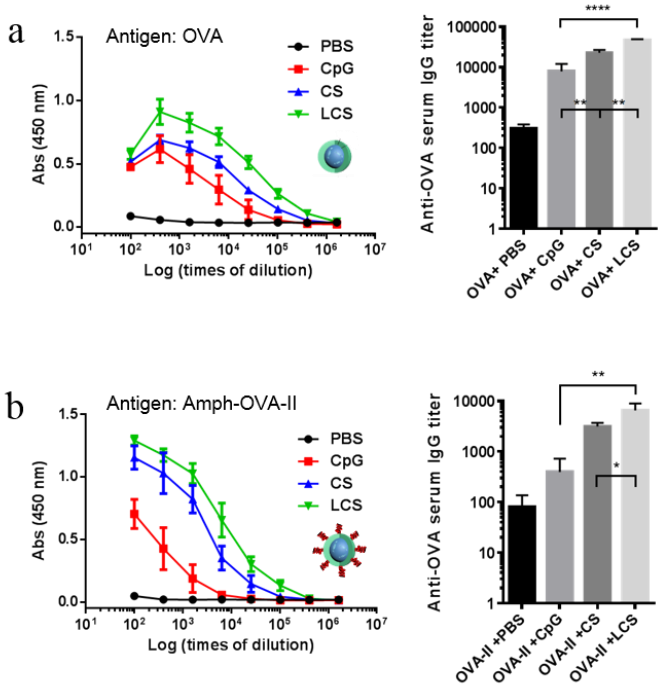

Figure 2-13. Anti-OVA IgG were measured by ELISA, a) Groups of C57BL/6 mice (n=3 per group) were immunized subcutaneously on day 0 and day 14 with 10 mg OVA and 1.24 nmol CpG DNA, CS, and LCS. b) Groups of C57BL/6 mice (n=3 per group) were immunized subcutaneously on day 0 and day 14 with 10 mg DSPE-PEG-OVA-II and 1.24 nmol CpG DNA, CS, and LCS.

2.3.7. SiNPs vaccination elicit a protective anti-tumor immune response.

Several studies have previously shown that in the EG.7-OVA murine lymphoma model, CpG DNA vaccination resulted in significant regression of tumor growth.[44, 77-82] Therefore, we next compared the anti-tumor vaccine adjuvant activities of CpG DNA in nanoparticle form by therapeutically vaccinating C57BL/6 mice bearing OVA-expressing EG.7 thymoma tumors with no treatment group. A total of 2×10^6 EG.7-OVA cells were subcutaneously inoculated into mice. When the tumor mass became palpable (7-8 mm), mice with established EG.7-OVA tumors were vaccinated on day 5, 11, and 18 with 20 μg OVA plus 1.24 nmol CpG DNA in nanoparticle form or controls. Nanoparticle delivery containing amph-OVA-II suppressed tumor growth in the early stage, but differences over the control condition were lost with time. The CpG DNA in both nanoparticle form plus OVA protein resulted in similar tumor initiation on day 7 as no treatment group, but delayed tumor growth significantly over time. The corresponding survival rate also supports the potential utility of our nanoparticle strategy for prophylactic cancer vaccines (Figure 2-14b). Notably, 2 or 3 mice showed a drastic inhibition of tumor growth and full recovery from OVA plus CS or OVA plus LCS group (Figure 2-14c and d). The nanoparticle-adjuvanted vaccine are more effective than soluble CpG DNA in stimulating tumor-specific cytotoxic T cells responses.

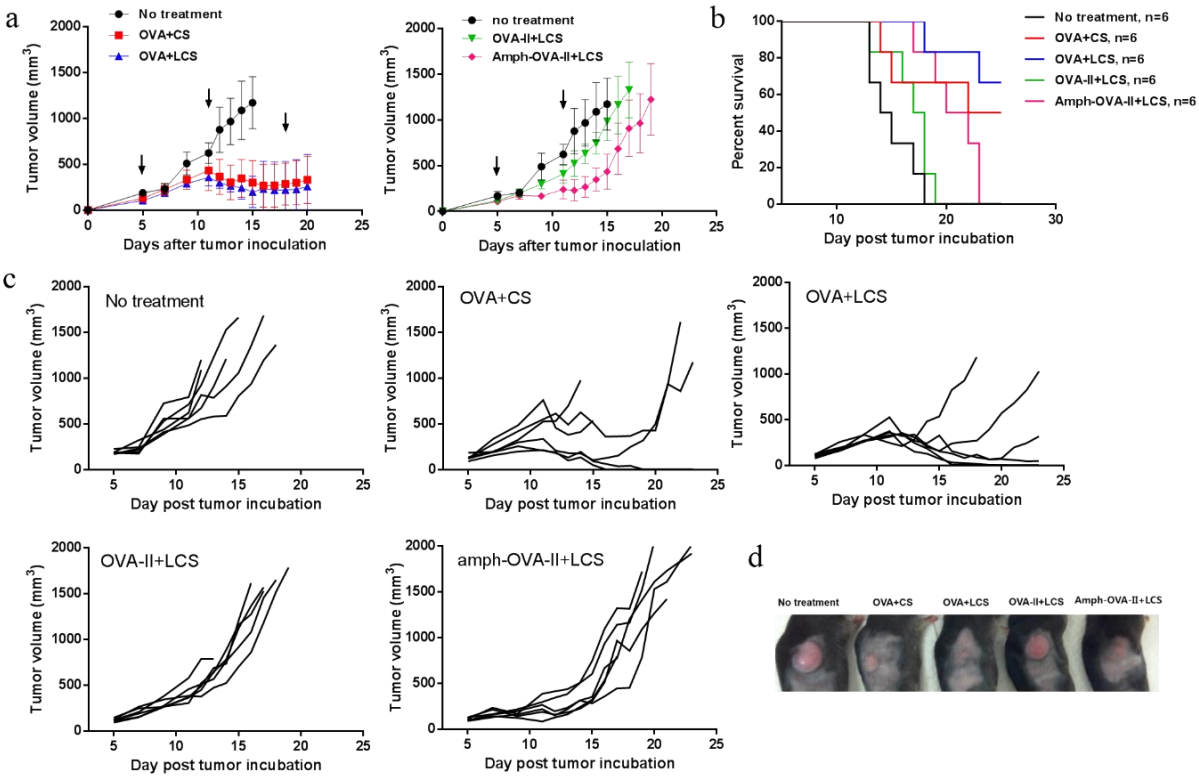

Figure 2-14. C57BL/6 mice (n=6 per group) were inoculated with 2 × 10^6 EG.7-OVA cells s.c. on day 0 and then vaccinated with 20 ug OVA mixed with 1.24 nmol SiNPs based CpG formulation on days 5, 11, and 18. a) tumor size over time. b) survival over time. c) individual tumor growth curves. d) An image represents the progression in tumor volume on day 15.

2.4. Conclusion

We used SiNPs as a platform for the efficient delivery of CpG DNA into dLNs for ensuring their immunostimulatory activity. This approach provides rapid and simple guidelines to fabricate effective vaccine carriers and understanding how the electrostatic charge interaction affects their vaccine loading, size, and surface charge. The optimum weight ratio between SiNPs and CpG DNA was explored, showing their high colloidal stability and efficient CpG DNA loading with minimal leakage into the medium. For better retention of CpG DNA in

nanoparticle form (CS), nanoparticles were coated with lipid bilayer, showing their better stability, enhanced delivery of CpG DNA to lymphatics, and cellular uptake efficiency. Immunization by nanoparticle delivery generated potent cellular and humoral immunity superior to vaccination by soluble CpG DNA. Nanoparticle delivery acts synergistically in suppressing tumor volume, outperforming the delivery of CpG DNA in animal model. Lipid coated silica nanoparticles revealed in this study can be used as efficient carriers to target vaccine adjuvants to dLNs, thereby modulating the immune system in safer and effective ways. We expect that the results of our work will contribute to the advancement of vaccine encapsulations via charge interactions and will help to develop more efficient therapeutics for treating cancer.

3. Dissolving microneedle arrays for transdermal delivery of molecular vaccines

3.1. Introduction

Delivery of vaccines via the skin is not a new phenomenon. Transdermal delivery through chemical permeation of the skin has advantages over hypodermic injections, which are painful, generate dangerous medical waste and spread of disease known to occur through needle-reuse. [83, 84] Many studies report a connection between unsafe needle-reuse and the transmission of infectious agents including hepatitis C virus (HCV), hepatitis B virus (HBV), or human immunodeficiency virus (HIV).[85] This needle-based injection also requires refrigeration that increases costs and complexity of cold transportation (the "cold chain"), and requires trained health care personnel.[86] Meanwhile, transdermal vaccine delivery systems represent noninvasive, potentially allowing for pain-free administration either by minimally trained health care providers or through self-administration. This system may improve safety for the vaccinator by reducing the generation of dangerous medical waste and inhibiting the spread of disease by needle re-use and needle-based injuries. However, transdermal vaccine delivery has yet to achieve its potential as an alternative to hypodermic injections. Perhaps only a limited number of vaccines or difficulties of controlled vaccine release are major hurdles to practical administration.[87] With current delivery systems, successful transdermal vaccines have molecular masses that are only up to a few hundred Daltons.[83, 88] It has been difficult to deliver hydrophilic vaccines such as DNA or small-interfering RNA (sRNA) with antigen peptides. Therefore, an optimal approach for safe, convenient administration of molecular-based adjuvants with antigen peptides through t he skin remains elusive.

Here we combined the transdermal vaccine delivery with an 'albumin hitchhiking'[63, 89] approach that uses albumin binding lipids conjugates for the efficient delivery of vaccines consisting CpG DNA and antigens into dLNs to ensure their immunostimulatory activity. We first designed microneedle arrays (MNs) composed of a biocompatible polymer (poly(acrylic acid), PAA), and used them for rapid release of encapsulated vaccine components into epidermis. The MNs is a glassy hard solid, which has enough strength (Young's modulus, E ≈ 4 GPa)[90] to penetrate the skin and water soluble, facilitating its rapid dissolution when inserted into skin. To show the utility of this approach, model vaccines composed of peptide antigen and diacyl lipid-CpG conjugate adjuvants (amph-vaccines) were loaded in MNs and administered in animal models. Due to the albumin binding nature of amph-vaccines, they form a complex of appropriate size through binding to albumin, and enhance their efficient drainage to lymphatics.[63] Previous results showed 10-fold higher accumulation in lymph nodes, 30-fold increases in T cell priming, and enhanced anti-tumor efficacy following subcutaneous administration.[63] In this study, use of MNs platform to deliver amph-vaccines resulted in enhanced antigen-specific T cell and antibody responses related to traditional needle-based immunization. This 'albumin hitchhiking' MNs delivery system can provide a simple and safer vaccination method with improved immunogenicity. We hypothesized that benefits of applying this platform are (i) safe and needle-free administration (no waste of biological waste and sharp disposal), (ii) no pain and needle phobia, leading to poor patient compliance, (iii) enhanced immune response through inflammatory cues and targeted delivery of amph-vaccines to response-governing antigen presenting cells (APCs) present at high density in the lymph nodes.

3.2. Background

Our skin consists of three layers such as epidermis, dermis and subcutaneous fat layer.[83, 91, 92] In addition, there is an external physical barrier called the stratum corneum. Methods of transdermal permeation include hydration, mechanical disruption, and a combination of the two. It was found that the rate of water loss from skin increased dramatically when the stratum corneum was removed.[88] Hydration of the stratum corneum with inflammatory cue causes keratinocytes to swell and fluid to pool in the intercellular spaces. This process allows antigens to pass the skin barrier more easily.[93, 94] For such barrier-disruption systems, a si mple application of MNs can be desired for physical or chemical disruption of the stratum corneum. Once they penetrate the skin, where immuno-component dendritic cells are densely distributed, skin permeability could be increased, allowing for trans dermal delivery of large molecules.[95] Ease of administration is also an advantage si nce rapid and pain-free self-administration of therapeutics into the skin could be app lied.

Delivery from hypodermal administration results in the compound being deposited either intramuscularly (IM), subcutaneously (SC), or intradermally (ID). As capable of transporting nano-sized molecules are available, the larger length scales of needles are often unnecessary, causing pain and limit targeted delivery. MNs has ~500 μm length, which is enough to penetrate epidermis. The skin's pain receptors are located slightly deeper than the length of MNs so that the delivery using MNs is pain-free in comparison to hypodermic needles. Due to these property, therapeutics can be delivered precisely into the epidermis without pain or discomfort.

MNs are specifically designed and developed according to their use and needs.[91] Solid MNs often used to pretreat the skin prior to the administration of therapeutics. It is also used

to deliver microgram quantities of the substance which may not be suitable for controllable delivery and could pose disposal or re-use hazards.[92] Vaccine-coated and hollow MNs are used for drug dissolution in the skin. Hollow MNs allows their drug diffuse in deeper later. Nonetheless, their application is limited as the risk of needle breakage for the injection of vaccine solutions and also they may leave sharp wastes. Thus, dissolving MNs were developed as a solution to safety and sharp waste issues. These MNs undergo complete dissolution in the skin and are typically made of water soluble polymer that dissolve once exposed to the skin.

3.3. Materials and methods

3.3.1. DNA Synthesis and lipophilic conjugation

All reagents for DNA synthesis were purchased from Chemgenes. G_2-CpG (5'-GGTCCATGACGTTCCTGACGTT-3') was first synthesized using an ABI 394 synthesizer (Applied Biosystems) on a 1.0 micromole scale. Lipophilic phosphoramidite was conjugated as a final 'base' on the 5' end of G_2-CpG (Lipo-G_2-CpG[63]). In this process, lipophilic phosphoramidite was dissolved in dichloromethane and coupled to G_2-CpG using the so-called syringe synthesis technique or using the DNA synthesizer [63]. After the synthesis, Lipo-G_2-CpG was cleaved form the solid support by AMA solution (methylamine:acetic acid=50:50) at 65 ^{o}C, and purified by reverse phase high performance liquid chromatography (HPLC). The schematics of Lipo-G_2-CpG is illustrated in Figure 3-1.

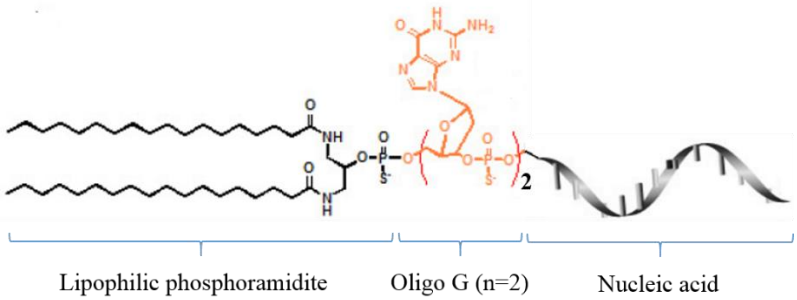

Figure 3-1. Structure of synthesized diacyl lipid conjugated CpG ODN (Lipo-G_2-CpG).

3.3.2. Synthesis of peptide amphiphile

Maleimide-polyethylene glycol $(PEG)_{2000}$-DSPE (Laysan Bio) and OVA-II peptide (Genescript) were dissolved in Dimethylformamide (DMF) separately. They were mixed together in the ratio of 2:1 chemical equivalent and small amount of Triethylamine (TEA) was added for their coupling. The mixture was agitated at 25 ºC for 24 hours. The coupling process and structure of DSPE-PEG_{2000}-OVA-II (amph-OVA-II) are described in Figure 3-2. The PEG spacer with optimized length between the albumin-binding tail and the OVA-II antigen was chosen to increase conjugate solubility as well as to promote albumin-binding.

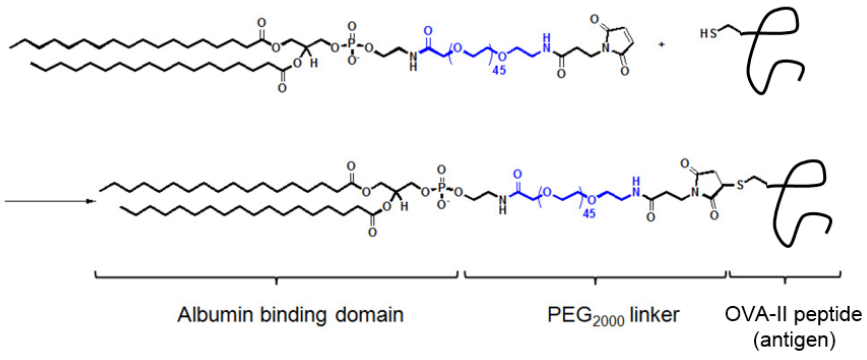

Figure 3-2. OVA-II peptide with amino-terminal cysteines were conjugated to maleimide-PEG_{2000}-DSPE.

3.3.3. Purification of synthesized DNA

Lipo-G_2-CpG was purified using reverse phase HPLC (Agilent Technologies 1220 Infinity LC) on a reverse phase C4 (BioBasic-4, 200 mm × 4.6 mm, Thermo Scientific) column. The mobile phase consisted of 100 mM trimethylamine-acetic acid buffer (TEAA, pH 7.5) and methanol (MeOH) as an eluent. The gradient linearity changed from 50:50 (MeOH:TEAA) to 0:100. The total run time was 20 min. The injection volume was 100 μl and Lipo-G_2-CpG was monitored using UV-Vis absorption. Data were collected using Agilent Rapid Res software.

3.3.4. Design and preparation of MNs

Silicone templates were purchased from Micropoint Technologies Pte Ltd. Templates were fabricated by casting room temperature vulcanizing silicon over a stainless microneedle master mold. The template has 10×10 array sharp cavities with 200 μm width and 500 μm height. They were used to build MNs delivery system through a simple fabrication process as shown in Figure 3-3a. The dissolving polymer was deposited to the template surface and centrifuged to compact them into template cavities. Following removal of residual material from the template surface, templates were dried at room temperature. In this process, vaccine components remained in not only MNs tips but also MNs body part (pedestal). To avoid this, the deposition process comprised two stages as shown in Figure 3-3b.

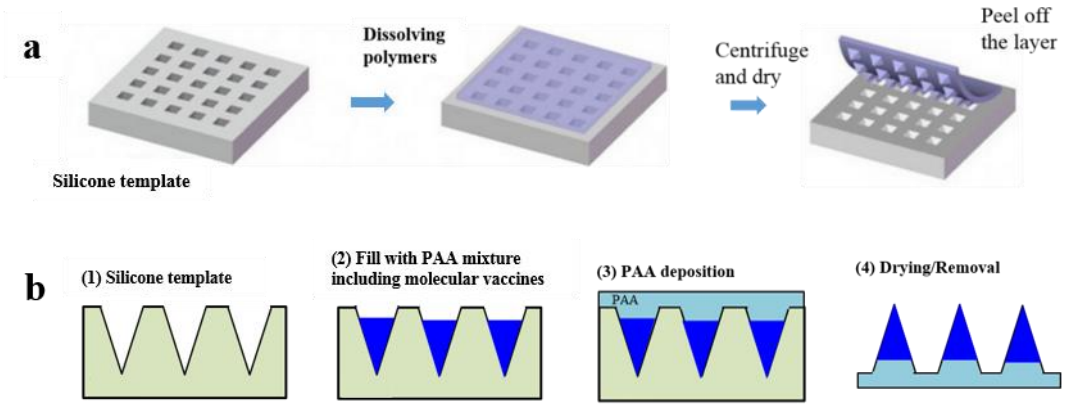

Figure 3-3. a) Schematic of simple dissolving microneedle fabrication. b) Fabrication of PAA MNs.

The template was cleaned first by washing with mild soap and letting them air dry completely, and small amount of PAA-vaccine solution was deposited onto the microneedle catchment. The PAA (250 kDa, 35 %) was added to soluble OVA and Lipo-G_2-CpG mixture at desired concentrations (generally ~ 40 mg/ml OVA, 32 mg/ml) to prepare the PAA-vaccine solution. The templates were centrifuged for 20 minutes at rcf ≈ 450 and excess PAA-vaccine solution was removed from the template surface for potential reuse. The templates containing PAA-vaccine were then dried at 25 ^{o}C for 24 hours. The PAA pedestals were formed via addition of 35 % PAA to the template surface, followed by centrifugation (20 min, rcf ≈ 450), the samples were dried at 25 ^{o}C for 48 h, before removing from the template.

3.3.5. Characterization of MNs

MNs were characterized by optical and confocal microscopy using a EVOS AMF4300 and a Zeiss LSM 510 respectively. The array morphology was further characterized by scanning electron microscopy (FE-SEM) using a JSM-7600 field effect-SEM and a JSM-6510LV SEM. Total vaccine loading was determined through brief exposure of fabricated arrays to

deionized water, followed by an ultraviolet-visible spectroscopy (UV-Vis).

3.3.6. In vivo MNs application and vaccine release

All animal studies were approved by the division of laboratory animal resources (DLAR) and animals were cared in the DLAR animal facility under federal, state, local, and NIH guidelines for animal care. The capability of MNs delivery system were tested on anesthetized C57BL/6 mice at the tail based area. Skin was rinsed briefly with PBS and dried before application of MNs by gentle pressure. After application, mice were euthanized at subsequent time points and the application site was dissected. Treated skin and MNs were imaged by confocal microscopy to assess transcutaneous delivery of PAA-vaccine implants. For histological analysis, excised skin was embedded in optimal cutting temperature medium (OCT, Tissue-Tek) and used for sectioning on cryostat (Thermo Fisher HM525 NX). Histological sections were then imaged using an EVOS AMF4300 imager.

3.3.7. Immunizations

Groups of C57BL/6 mice (n=3 per group) were immunized by ID injection or by MNs patch (5 min application) on day 0 and day 14 with 10 μg ovalbumin (OVA) including Lipo-G_2-CpG formulations as shown in Figure 3-4a. Groups from 1 to 3 were selected as control groups to compare immune responses from MNs application with that from ID injections as shown in Figure 3-4b. Seven days after the final immunization, mice were bled and peripheral blood mononuclear cells were evaluated by SIINFEKL/H-2Kb peptide-MHC tetramers staining and intracellular cytokine staining.

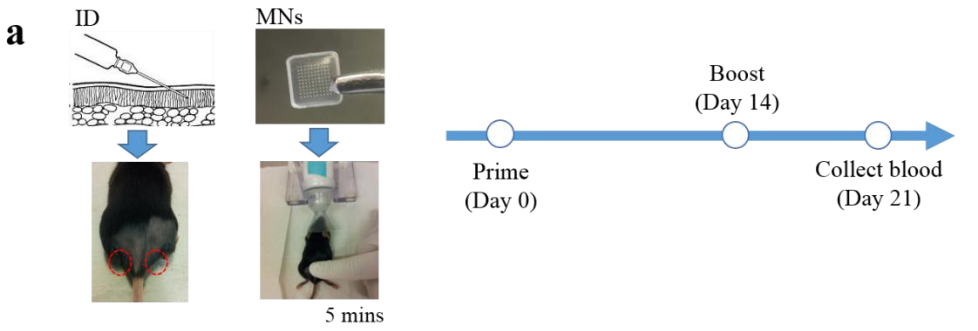

b

		Adjuvants and antigens
ID injection	Group 1	PBS + OVA
	Group 2	CpG + OVA
	Group 3	Lipo-G_2-CpG + OVA
MNs injection	Group 4	MNs (Lipo-G_2-CpG + OVA)

Figure 3-4. a) Mice immunization via ID injection or MNs delivery system (5 min application), and b) groups of C57BL/6 mice (n = 3 per group).

To assess the functionality of primed $CD8^+$ T cells, peripheral blood mononuclear cells were stimulated *ex vivo* with 10 µg/mL OVA peptide SIINFEKL for 6 h with Brefeldin-A and then fixed, permeabilized, stained with anti-IFN-γ, anti-TNF-α, and anti-CD8α, and analyzed by flow cytometry. Anti-ovalbumin IgG titers, defined as the dilution of serum at which 450 nm OD will be determined by an enzyme-linked immunosorbent assay (ELISA) analysis. To determine antibody titers, ELISA plates (eBioscience) were coated with 10 µg/mL of OVA peptide in PBS 1X overnight at room temperature. The plates were blocked with 200 µL of 1% BSA in PBS (FACS buffer) for 1 h. Serum was serially diluted in PBS 1X between 1:102 and 1:109 and applied to wells for 1 h at room temperature. Peroxidase-conjugated goat anti-mouse IgG (HþL) (1:5000 in 1% BSA-PBST, 100 µL/well) was then applied for 1 h, and the plates were developed using TMB substrate (100 µL/well, eBioscience). The reaction was stopped using 50 µL of 1 M sulfuric acid, 100 µL of the solution and absorbance values were measured at 450 nm.

3.3.8. Statistical analysis

To analyze the statistical difference between four groups, a One-Way Analysis of Variance (ANOVA) with Tukey's HSD post-hoc test was used. All of the values are expressed as means ± standard deviations. GraphPad Prism software was used for all the statistical analyses. ****P<0.0001, ***P<0.001, **P<0.01, *P<0.05. NS, not significant.

3.4. Results and Discussion

3.4.1. Preparation of MNs

We first designed microneedle geometry and device fabrication process to encapsulate vaccine components in tips of MNs. To facilitate reliable insertion of MNs into skin, each was designed to be 500 μm long, which can provide sufficient mechanical strength. To prepare vaccine loaded MNs, we pursued a double-layered MNs design (Figure 3-3b) using PAA polymers. First, the PAA solution (250 kDa, 35 %) was mixed with OVA plus TLR9 agonist diacyle lipid conjugated oligo guanine (n=2) repeated CpG DNA (amph-CpG) to prepare PAA-vaccine solution. Silicone templates were then cast with small amount of PAA-vaccine (≈ 5 μl) solution and centrifuged to infiltrate the template cavities. After removing excess PAA-vaccine solution, templates were allowed to dry at room temperature overnight to form solid vaccine loaded PAA tips within cavities of templates. Following the dry process, 35 % PAA was added to the template surface and centrifuged to compact the PAA into the cavities to form PAA pedestal structure. MNs were dried in the template at room temperature for 48 h (at least 24 h) and removed for future MNs applications (Figure 3-5a).

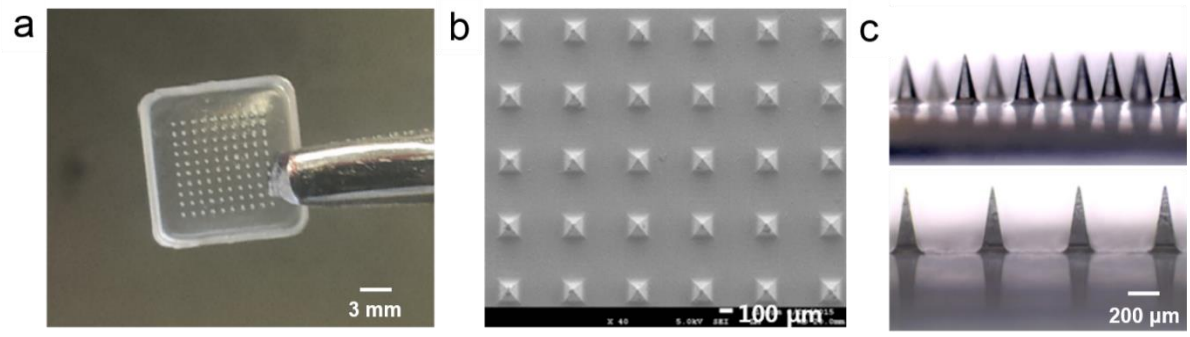

Figure 3-5. (a) Face view of dissolving PAA MNs. (b) SEM images of resulting MNs (scale bar 100 µm) and (c) side view of MNs.

The resulting MNs were reliably produced repeatedly and measured 500 µm tall with sharp tips as shown in FE-SEM and optical microscope images in Figure 3-5b and c. We further confirmed this MNs using confocal microcopy to observe the localization of the vaccine cargo in the tips.

2.4.2. Insertion and dissolution of MNs in skin

The resulting MNs were able to be inserted into murine skin of C57BL/6 mice with gentle force applied by the thumb (Figure 3-6a and b). To confirm release kinetics of encapsulated vaccines in MNs, we fabricated rhodamine dye loaded MNs and applied these arrays to the murine skin for 5 minutes. Confocal imaging on excised skin where patches were applied represented overlaid punctate fluorescent signal from rhodamine dye at individual sites of microneedle insertion. It indicates the effective delivery of PAA-loaded vaccine components upon microneedle penetrations into the cutaneous space (Figure 3-6b). Confocal imaging of MNs before and after application revealed complete loss of PAA-associated rhodamine dye signal from the length of each microneedle (Figure 3-6c). We further observed the loss of tips that were probably dissolved in the skin (Figure 3-6d and e). Upon insertion into murine

skin, MNs penetrated to a depth of approximately 150 μm and deposited their encapsulated rhodamine largely within the epidermis (Figure 3-6f).

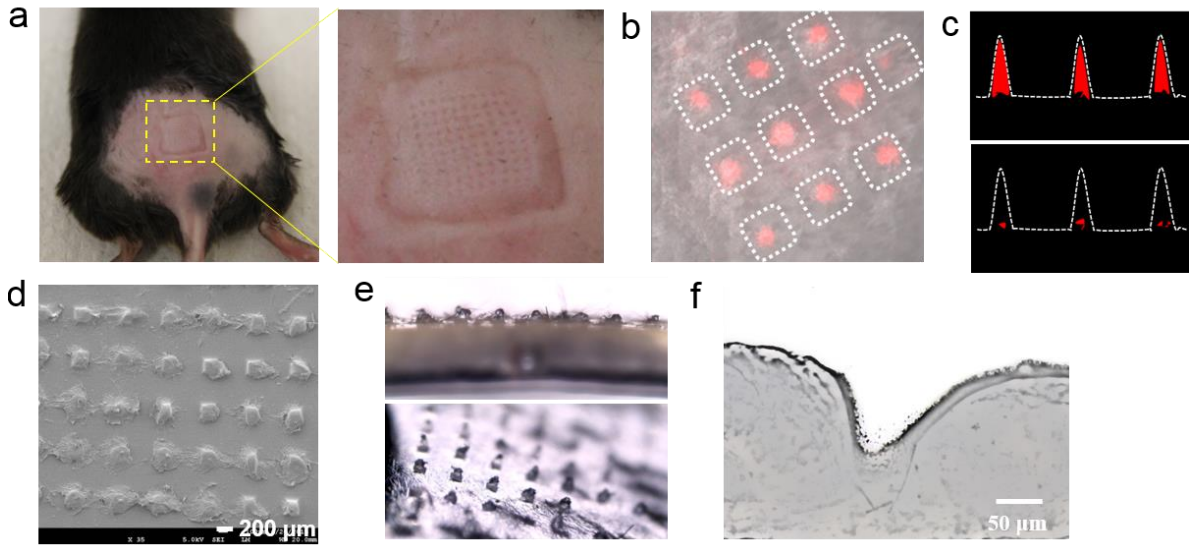

Figure 3-6. (a) En face view of murine skins after insertion and removal of MNs. (b) Confocal microscopy image of skins, showing deposition of rhodamine at needle penetration sites directly following MNs application for 5 min. (c) Confocal microscopy image before application (upper) and following a 5 min application to murine skin. (d) SEM image and (e) side views of MNs after applications. (f) Histological structure of mammalian skin after MNs application.

Together these results confirm MNs can effectively penetrate into murine skin with rapid dissolution of PAA-vaccine tips upon exposure to skin fluids. Once they penetrate the sk in, skin permeability could be increased, allowing for targeted delivery of antigen a nd adjuvant to LNs.

3.4.3. MNs vaccination

The efficacy of skin immunization with dissolving MNs was determined in C57BL/6 mice that received encapsulated amph-vaccines. For comparison to parenteral administration, we performed ID injection of dose-matched OVA plus soluble CpG or amph-CpG formulations in the murine skin. Mice were immunized on day 0 and boosted on day 14 with 10 μg OVA plus 1.24 nmol CpG or amph-CpG by ID injection or by MNs administration at the tail base. The cellular immunity was monitored by measuring OVA-specific $CD8^+$ T cell proliferation in peripheral blood using SIINFEKL/H-2Kb peptide-MHC tetramers. In view of the results shown in Figure 3-7, ID injected soluble CpG induced extremely weak antigen-specific $CD8^+$ T cell responses while ID injected amph-CpG elicited stronger $CD8^+$ T cell proliferation. This amph-CpG promotes binding to albumin in the interstitium and accumulates in antigen presenting cells in the LNs via albumin trafficking pathways, in turn lead to greatly improved immune responses as a lymph-directed vaccine carrier.[96] Increased access to the lymph and LNs promotes antigen processing with immune cells compared to free vaccine. MNs vaccination carrying amph-CpG also showed higher level of $CD8^+$ T cell proliferation, suggesting MNs delivery provided similar initial immunogenicity compared with traditional parenteral immunization strategies. We also evaluated the functionality of these expanded T cells through detection of inflammatory cytokine production following re-stimulation of peripheral blood mononuclear cells on day 21 ex vivo with SIINFEKL peptide. Flow cytometric analysis from intracellular staining indicated high frequencies of antigen-dependent functional cytokine-secreting $CD8^+$ T cells by MNs vaccination. These results suggest that MNs delivery can generate a higher frequency of $CD8^+$ T cells producing both IFN-γ and TNF-α, which are critical for innate and adaptive immunity against viral infections.[72]

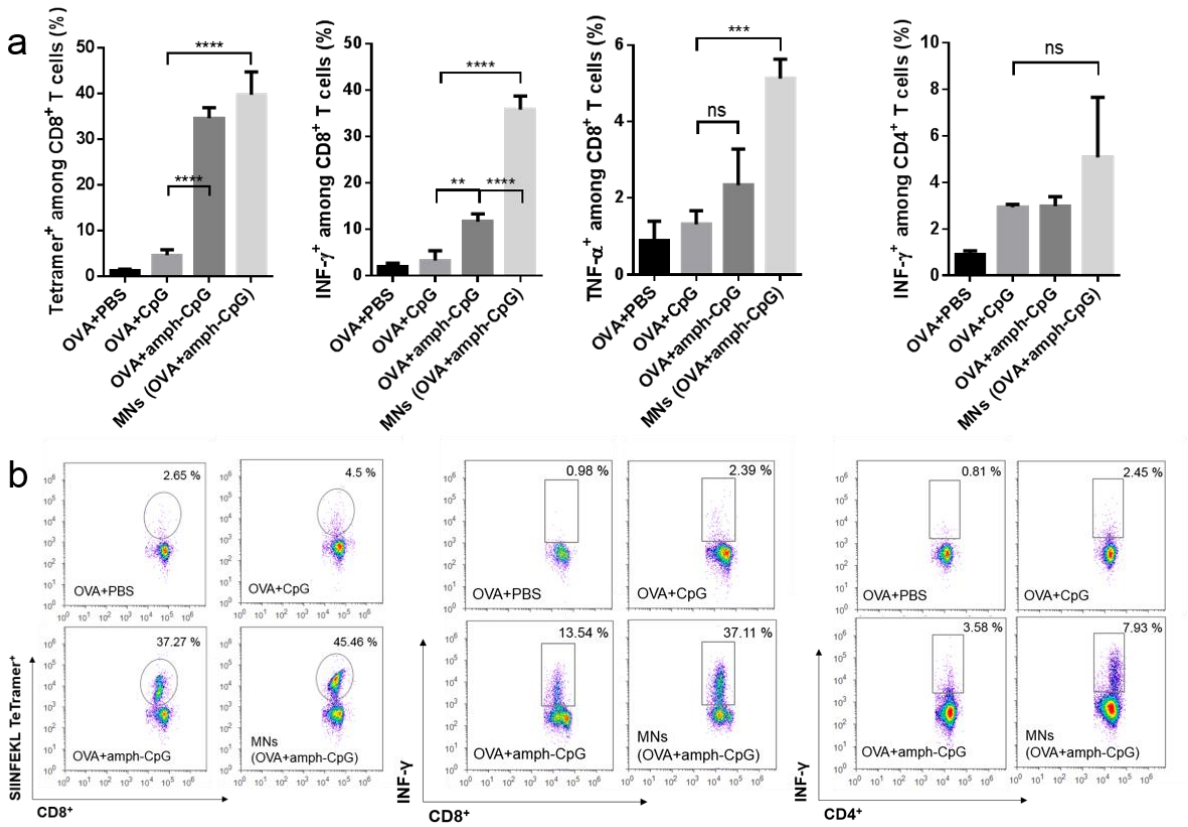

Figure 3-7. a) Frequency of tetramer^{+} CD8^{+} T cells in peripheral blood producing IFN-γ and TNF-α, and CD4^{+} T cells producing IFN- γ following SIINFEKL restimulation assessed by flow cytometry. b) Representative flow cytometric dot plots.

Additionally, we evaluated the functional capacity of lymph node targeting CD4 epitope (amph-OVA-II) elicited T cell response through detection of IFN-γ production following re-stimulation of peripheral blood mononuclear cells on day 21 with OVA-II peptide (Figure 3-8). The results revealed enhanced cytokine production by CD4^{+} T cell can be induced by MNs administration of amph-vaccines for specific antigen dependent production of IFN-γ.

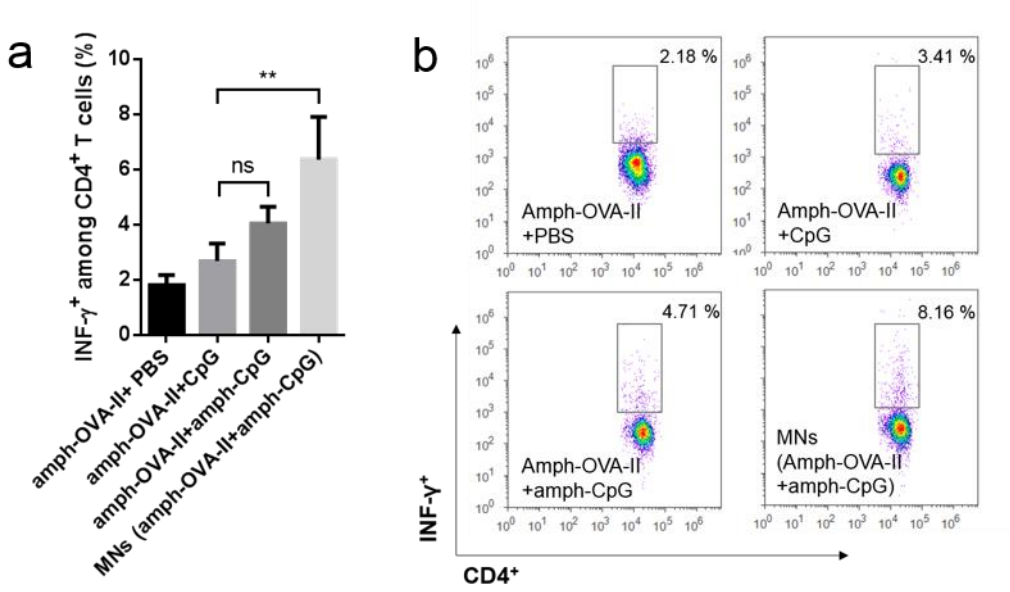

Figure 3-8. Groups of C57BL/6 mice (n=3 per group) were immunized subcutaneously on day 0 and day 14 with 10 μg amph-OVA-II plus 1.24 nmol CpG or amph-CpG by ID or MNs vaccination.

Finally, we measured the level of OVA-specific IgG in the sera of immunized mice to compare the capacity of generating humoral immunity. Measurement of the IgG level gives insight into the types of T helper cell immune responses. It was reported that the immune system responds to CpG motifs which is part of CpG ODN by activating potent Th1-like immune responses.[21] To evaluate the antibody response elicited by ID or MNs vaccination, we collected sera from immunized mice on day 21 following a prime on day 0 and boost on day 14 by ID or MNs vaccination. Here, ELISA measurements of serum titers of OVA-specific IgG showed the presence of similarly high levels of anti-OVA IgG in mice immunized by ID and MNs administration of amph-CpG (Figure 3-9a). When animals were immunized by amph-OVA-II plus amph-CpG formulation, MNs induced significant increases in serum titers for anti-OVA IgG (Figure 3-9b), similar to amphiphilic vaccines with ID injection.

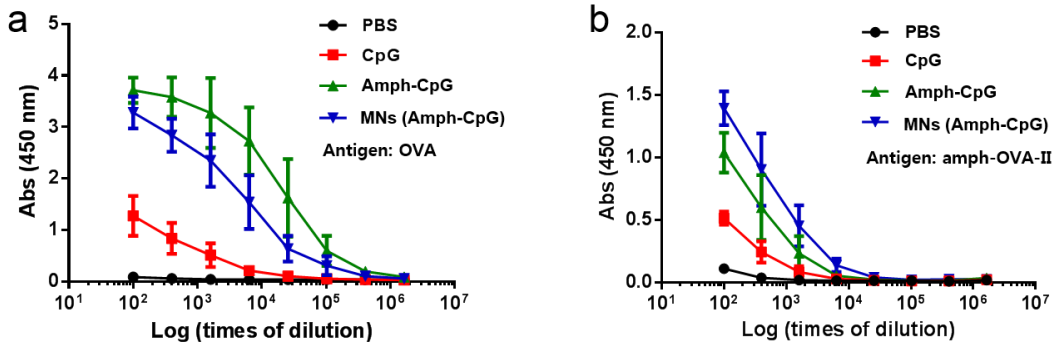

Figure 3-9. Anti-OVA IgG were measured by ELISA, a) Groups of C57BL/6 mice (n=3 per group) were immunized on day 0 and day 14 with 10 μg OVA plus 1.24 nmol CpG or amph-CpG by ID or MNs vaccination. b) Groups of C57BL/6 mice (n=3 per group) were immunized on day 0 and day 14 with 10 μg amph-OVA-II plus 1.24 nmol CpG or amph-CpG by ID or MNs vaccination.

These increases in the magnitude of cellular immune responses suggest that MNs delivery can provide systemic dispersion of amph-vaccines released upon skin insertion and plays a critical role in the adaptive cellular immune response. These results demonstrated the effectiveness of using MNs as a route for delivering "albumin hitchhiking" vaccines. Immunization through skin may target vaccine compounds to innate dendritic cells directly via lymphatic from proximal dLNs in parallel with activating the rich dendritic cell populations that reside in skin (Figure 3-10). The physical disruption of the epidermal/dermal tissues during MNs delivery is also considered to be a pivotal role in mediating enhanced immunity via the recruitment and maturation of APCs.[97, 98]

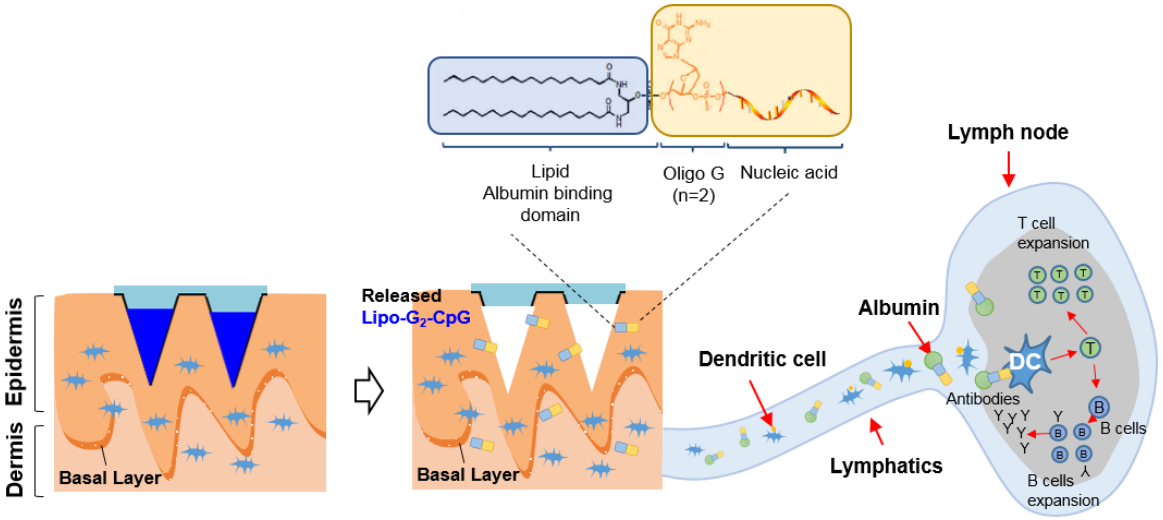

Figure 3-10. Schematic diagram of 'albumin hitchhiking' MNs delivery system in relation to immunology of the skin. The amph-vaccines and antigen internalized dendritic cells traffic to local lymph nodes to induce an immune response related to T and B cells.

3.5. Conclusions

We have demonstrated the utility of MNs designed for the systemic dispersion of amph-vaccines released upon skin insertion. This approach can provide a number of safety and immunological advantages compared to hypodermic needles. First, dissolving MNs generate no biohazardous sharp wastes because the MNs dissolve and disappear upon insertion. The pedestal part of MNs is also made of water-soluble polymer so that it can easily be eliminated by dissolving in water. [99] This safety feature removes the risk of accidental needle-stick injury or intentional reuse of needles, which is common in some developing countries and is responsible for close to one million deaths per year due to transmission of hepatitis B, HIV and other infectious diseases.[100] Second, the MNs delivery enhances the immune response through inflammatory cues and targeted delivery of antigen and adjuvant to high density of APCs in LNs. This approach can greatly increase the safety profile of administered vaccines by effectively guiding them to dLNs, reducing systemic dissemination.

In conclusion, ‘albumin hitchhiking’ MNs delivery system may provide not only practical advantages compared to hypodermic needles but also better humoral and cellular immunity. This strategy can be used as an effective platform for straightforward and robust transcutaneous vaccine delivery.

4. Conclusion and future work

We have designed and characterized a system for vaccine delivery that utilizes several advantages of nanoparticles: surface display of antigen, efficient lymphatic drainage, and versatile packaging of immunomodulating adjuvants via strong electrostatic surface charge interactions and T-helper peptides through a membrane post insertion method. We used lipid coated SiNPs as a platform for the efficient delivery of CpG DNA into dLNs for ensuring their immunostimulatory activity. This approach showed enhanced delivery of CpG DNA to lymphatics, and cellular uptake efficiency. Immunization by nanoparticle delivery generated potent cellular and humoral immunity superior to vaccination by soluble CpG DNA. In addition, nanoparticle delivery demonstrated improved therapeutic benefits in suppressing tumor growth, outperforming soluble CpG DNA in animal model. We expect that lipid coated silica nanoparticles can be used as efficient carriers to target vaccine adjuvants to dLNs, thereby modulating the immune system in safer and effective ways.

We have also demonstrated the utility of transdermal delivery platforms (microneedle arrays (MNs)) designed for the systemic dispersion of amph-vaccines released upon skin insertion. This approach showed a number of safety and immunological advantages compared to hypodermic needles. MNs delivery enhanced the immune response through inflammatory cues and targeted delivery of antigen and adjuvant to high density of APCs in LNs. This strategy can provide not only practical advantages compared to hypodermic needles but also better humoral and cellular immunity.

Although we observed enhanced efficacy and safety in mice with lipid-coated SiNPs, there are several important features that have not been addressed in this thesis. For example, the vaccine kinetics was not fully controlled by our current method. Future studies might focus on how to maximize the efficacy of adjuvant immunotherapy by controlling the kinetics of

vaccines exposure in LN. We are currently exploring the possibility of combining nanoparticle with layer by layer technique to achieve the kinetics control. Additionally, microneedle arrays might be an ideal approach to facilitate the layer-by-layer delivery of nanoparticles with kinetic control.

REFERENCES

1. Torre, L. A.; Bray, F.; Siegel, R. L.; Ferlay, J.; Lortet-Tieulent, J.; Jemal, A., Global cancer statistics, 2012. *CA: A Cancer Journal for Clinicians* **2015,** 65, (2), 87-108.

2. Ferlay, J.; Shin, H.-R.; Bray, F.; Forman, D.; Mathers, C.; Parkin, D. M., Estimates of worldwide burden of cancer in 2008: GLOBOCAN 2008. *International Journal of Cancer* **2010,** 127, (12), 2893-2917.

3. Formenti, S. C.; Demaria, S., Combining Radiotherapy and Cancer Immunotherapy: A Paradigm Shift. *Journal of the National Cancer Institute* **2013**.

4. Group, G. T. S., Treatment of Locally Unresectable Carcinoma of the Pancreas: Comparison of Combined-Modality Therapy (Chemotheraphy Plus Radiotherapy) to Chemotheraphy Alone1. *Journal of the National Cancer Institute* **1988,** 80, (10), 751-755.

5. Lu, W.; Arraes, L. C.; Ferreira, W. T.; Andrieu, J.-M., Therapeutic dendritic-cell vaccine for chronic HIV-1 infection. *Nat Med* **2004,** 10, (12), 1359-1365.

6. Banchereau, J.; Palucka, A. K.; Dhodapkar, M.; Burkeholder, S.; Taquet, N.; Rolland, A.; Taquet, S.; Coquery, S.; Wittkowski, K. M.; Bhardwaj, N.; Pineiro, L.; Steinman, R.; Fay, J., Immune and Clinical Responses in Patients with Metastatic Melanoma to CD34+ Progenitor-derived Dendritic Cell Vaccine. *Cancer Research* **2001,** 61, (17), 6451-6458.

7. June, C.; Rosenberg, S. A.; Sadelain, M.; Weber, J. S., T-cell therapy at the threshold. *Nat Biotech* **2012,** 30, (7), 611-614.

8. Vonderheide, R. H.; June, C. H., Engineering T cells for cancer: our synthetic future. *Immunological Reviews* **2014,** 257, (1), 7-13.

9. June, C.; Maus, M.; Plesa, G.; Johnson, L.; Zhao, Y.; Levine, B.; Grupp, S.; Porter, D., Engineered T cells for cancer therapy. *Cancer Immunology, Immunotherapy* **2014,** 63, (9), 969-975.

10. Naidoo, J.; Page, D. B.; Wolchok, J. D., Immune Checkpoint Blockade. *Hematology/Oncology Clinics of North America* **2014,** 28, (3), 585-600.

11. Topalian, Suzanne L.; Drake, Charles G.; Pardoll, Drew M., Immune Checkpoint Blockade: A Common Denominator Approach to Cancer Therapy. *Cancer Cell* **2015,** 27, (4), 450-461.

12. Postow, M. A.; Callahan, M. K.; Wolchok, J. D., Immune Checkpoint Blockade in Cancer Therapy. *Journal of Clinical Oncology* **2015,** 33, (17), 1974-1982.

13. Jeanbart, L.; Swartz, M. A., Engineering opportunities in cancer immunotherapy. *Proceedings of the National Academy of Sciences* **2015,** 112, (47), 14467-14472.

14. Rosenberg, S. A.; Yang, J. C.; Restifo, N. P., Cancer immunotherapy: moving beyond current vaccines. *Nat Med* **2004,** 10, (9), 909-915.

15. Krieg, A. M., Therapeutic potential of Toll-like receptor 9 activation. *Nat Rev Drug Discov* **2006,** 5, (6), 471-484.

16. Iwasaki, A.; Medzhitov, R., Regulation of Adaptive Immunity by the Innate Immune System. *Science* **2010,** 327, (5963), 291-295.

17. Weng, N.-p., Aging of the Immune System: How Much Can the Adaptive Immune System Adapt? *Immunity* **2006,** 24, (5), 495-499.

18. Solana, R.; Pawelec, G.; Tarazona, R., Aging and Innate Immunity. *Immunity* **2006,** 24, (5), 491-494.

19. Takeuchi, O.; Akira, S., Pattern Recognition Receptors and Inflammation. *Cell* **2010,** 140, (6), 805-820.

20. Iwasaki, A.; Medzhitov, R., Toll-like receptor control of the adaptive immune responses. *Nat Immunol* **2004,** 5, (10), 987-995.

21. Krieg, A. M.; Yi, A.-K.; Matson, S.; Waldschmidt, T. J.; Bishop, G. A.; Teasdale, R.; Koretzky, G. A.; Klinman, D. M., CpG motifs in bacterial DNA trigger direct B-cell activation.

Nature **1995,** 374, (6522), 546-549.

22. Klinman, D. M.; Yi, A. K.; Beaucage, S. L.; Conover, J.; Krieg, A. M., CpG motifs present in bacteria DNA rapidly induce lymphocytes to secrete interleukin 6, interleukin 12, and interferon gamma. *Proceedings of the National Academy of Sciences* **1996,** 93, (7), 2879-2883.

23. Stern, B. V.; Boehm, B. O.; Tary-Lehmann, M., Vaccination with Tumor Peptide in CpG Adjuvant Protects Via IFN-γ-Dependent CD4 Cell Immunity. *The Journal of Immunology* **2002,** 168, (12), 6099-6105.

24. Krieg, A. M., CpG motifs: the active ingredient in bacterial extracts? *Nat Med* **2003,** 9, (7), 831-835.

25. Krieg, A. M., CPG MOTIFS IN BACTERIAL DNA AND THEIR IMMUNE EFFECTS. *Annual Review of Immunology* **2002,** 20, (1), 709-760.

26. Girard, J.-P.; Moussion, C.; Forster, R., HEVs, lymphatics and homeostatic immune cell trafficking in lymph nodes. *Nat Rev Immunol* **2012,** 12, (11), 762-773.

27. Yang, X.; Yang, M.; Pang, B.; Vara, M.; Xia, Y., Gold Nanomaterials at Work in Biomedicine. *Chemical Reviews* **2015**.

28. Irvine, D. J.; Hanson, M. C.; Rakhra, K.; Tokatlian, T., Synthetic Nanoparticles for Vaccines and Immunotherapy. *Chemical Reviews* **2015,** 115, (19), 11109-11146.

29. Mehta, N. K.; Moynihan, K. D.; Irvine, D. J., Engineering New Approaches to Cancer Vaccines. *Cancer Immunology Research* **2015,** 3, (8), 836-843.

30. Peer, D.; Karp, J. M.; Hong, S.; Farokhzad, O. C.; Margalit, R.; Langer, R., Nanocarriers as an emerging platform for cancer therapy. *Nat Nano* **2007,** 2, (12), 751-760.

31. Hu, C.-M. J.; Fang, R. H.; Copp, J.; Luk, B. T.; Zhang, L., A biomimetic nanosponge that absorbs pore-forming toxins. *Nat Nano* **2013,** 8, (5), 336-340.

32. Hu, C.-M. J.; Zhang, L.; Aryal, S.; Cheung, C.; Fang, R. H.; Zhang, L., Erythrocyte

membrane-camouflaged polymeric nanoparticles as a biomimetic delivery platform. *Proceedings of the National Academy of Sciences* **2011,** 108, (27), 10980-10985.

33. Hu, C.-M. J.; Fang, R. H.; Luk, B. T.; Zhang, L., Nanoparticle-detained toxins for safe and effective vaccination. *Nat Nano* **2013,** 8, (12), 933-938.

34. Copp, J. A.; Fang, R. H.; Luk, B. T.; Hu, C.-M. J.; Gao, W.; Zhang, K.; Zhang, L., Clearance of pathological antibodies using biomimetic nanoparticles. *Proceedings of the National Academy of Sciences* **2014,** 111, (37), 13481-13486.

35. Pang, Z.; Hu, C.-M. J.; Fang, R. H.; Luk, B. T.; Gao, W.; Wang, F.; Chuluun, E.; Angsantikul, P.; Thamphiwatana, S.; Lu, W.; Jiang, X.; Zhang, L., Detoxification of Organophosphate Poisoning Using Nanoparticle Bioscavengers. *ACS Nano* **2015,** 9, (6), 6450-6458.

36. Fang, R. H.; Luk, B. T.; Hu, C.-M. J.; Zhang, L., Engineered nanoparticles mimicking cell membranes for toxin neutralization. *Advanced Drug Delivery Reviews* **2015,** 90, 69-80.

37. Gao, W.; Fang, R. H.; Thamphiwatana, S.; Luk, B. T.; Li, J.; Angsantikul, P.; Zhang, Q.; Hu, C.-M. J.; Zhang, L., Modulating Antibacterial Immunity via Bacterial Membrane-Coated Nanoparticles. *Nano Letters* **2015,** 15, (2), 1403-1409.

38. Gao, W.; Thamphiwatana, S.; Angsantikul, P.; Zhang, L., Nanoparticle approaches against bacterial infections. *Wiley Interdisciplinary Reviews: Nanomedicine and Nanobiotechnology* **2014,** 6, (6), 532-547.

39. Hu, C.-M. J.; Fang, R. H.; Wang, K.-C.; Luk, B. T.; Thamphiwatana, S.; Dehaini, D.; Nguyen, P.; Angsantikul, P.; Wen, C. H.; Kroll, A. V.; Carpenter, C.; Ramesh, M.; Qu, V.; Patel, S. H.; Zhu, J.; Shi, W.; Hofman, F. M.; Chen, T. C.; Gao, W.; Zhang, K.; Chien, S.; Zhang, L., Nanoparticle biointerfacing by platelet membrane cloaking. *Nature* **2015,** 526, (7571), 118-121.

40. Fang, R. H.; Kroll, A. V.; Zhang, L., Nanoparticle-Based Manipulation of Antigen-

Presenting Cells for Cancer Immunotherapy. *Small* **2015,** 11, (41), 5483-5496.

41. Xu, Z.; Ramishetti, S.; Tseng, Y.-C.; Guo, S.; Wang, Y.; Huang, L., Multifunctional nanoparticles co-delivering Trp2 peptide and CpG adjuvant induce potent cytotoxic T-lymphocyte response against melanoma and its lung metastasis. *Journal of Controlled Release* **2013,** 172, (1), 259-265.

42. Xu, Z.; Wang, Y.; Zhang, L.; Huang, L., Nanoparticle-Delivered Transforming Growth Factor-β siRNA Enhances Vaccination against Advanced Melanoma by Modifying Tumor Microenvironment. *ACS Nano* **2014,** 8, (4), 3636-3645.

43. Zhao, Y.; Huo, M.; Xu, Z.; Wang, Y.; Huang, L., Nanoparticle delivery of CDDO-Me remodels the tumor microenvironment and enhances vaccine therapy for melanoma. *Biomaterials* **2015,** 68, 54-66.

44. Kim, S.-Y.; Heo, M. B.; Hwang, G.-S.; Jung, Y.; Choi, D. Y.; Park, Y.-M.; Lim, Y. T., Multivalent Polymer Nanocomplex Targeting Endosomal Receptor of Immune Cells for Enhanced Antitumor and Systemic Memory Response. *Angewandte Chemie International Edition* **2015,** 54, (28), 8139-8143.

45. He, Q.; Shi, J., Mesoporous silica nanoparticle based nano drug delivery systems: synthesis, controlled drug release and delivery, pharmacokinetics and biocompatibility. *Journal of Materials Chemistry* **2011,** 21, (16), 5845-5855.

46. Wang, Y.; Caruso, F., Template Synthesis of Stimuli-Responsive Nanoporous Polymer-Based Spheres via Sequential Assembly. *Chemistry of Materials* **2006,** 18, (17), 4089-4100.

47. Dengler, E. C.; Liu, J.; Kerwin, A.; Torres, S.; Olcott, C. M.; Bowman, B. N.; Armijo, L.; Gentry, K.; Wilkerson, J.; Wallace, J.; Jiang, X.; Carnes, E. C.; Brinker, C. J.; Milligan, E. D., Mesoporous silica-supported lipid bilayers (protocells) for DNA cargo delivery to the spinal cord. *Journal of Controlled Release* **2013,** 168, (2), 209-224.

48. Liu, X.; Situ, A.; Kang, Y.; Villabroza, K. R.; Liao, Y.; Chang, C. H.; Donahue, T.; Nel,

A. E.; Meng, H., Irinotecan Delivery by Lipid-Coated Mesoporous Silica Nanoparticles Shows Improved Efficacy and Safety over Liposomes for Pancreatic Cancer. *ACS Nano* **2016,** 10, (2), 2702-2715.

49. Meng, H.; Wang, M.; Liu, H.; Liu, X.; Situ, A.; Wu, B.; Ji, Z.; Chang, C. H.; Nel, A. E., Use of a Lipid-Coated Mesoporous Silica Nanoparticle Platform for Synergistic Gemcitabine and Paclitaxel Delivery to Human Pancreatic Cancer in Mice. *ACS Nano* **2015,** 9, (4), 3540-3557.

50. Liu, J.; Stace-Naughton, A.; Brinker, C. J., Silica nanoparticle supported lipid bilayers for gene delivery. *Chemical communications (Cambridge, England)* **2009**, (34), 5100-5102.

51. Tao, C.; Zhu, Y.; Li, X.; Hanagata, N., Binding of CpG oligodeoxynucleotides to mesoporous silica nanoparticles for enhancing delivery efficiency. *Microporous and Mesoporous Materials* **2015,** 204, 91-98.

52. Du, X.; Shi, B.; Tang, Y.; Dai, S.; Qiao, S. Z., Label-free dendrimer-like silica nanohybrids for traceable and controlled gene delivery. *Biomaterials* **2014,** 35, (21), 5580-5590.

53. Zhang, H.; Chen, S.; Zhi, C.; Yamazaki, T.; Hanagata, N., Chitosan-coated boron nitride nanospheres enhance delivery of CpG oligodeoxynucleotides and induction of cytokines. *International Journal of Nanomedicine* **2013,** 8, 1783-1793.

54. Hartono, S. B.; Phuoc, N. T.; Yu, M.; Jia, Z.; Monteiro, M. J.; Qiao, S.; Yu, C., Functionalized large pore mesoporous silica nanoparticles for gene delivery featuring controlled release and co-delivery. *Journal of Materials Chemistry B* **2014,** 2, (6), 718-726.

55. Nel, A. E.; Madler, L.; Velegol, D.; Xia, T.; Hoek, E. M. V.; Somasundaran, P.; Klaessig, F.; Castranova, V.; Thompson, M., Understanding biophysicochemical interactions at the nano-bio interface. *Nat Mater* **2009,** 8, (7), 543-557.

56. Leroueil, P. R.; Berry, S. A.; Duthie, K.; Han, G.; Rotello, V. M.; McNerny, D. Q.; Baker, J. R.; Orr, B. G.; Banaszak Holl, M. M., Wide Varieties of Cationic Nanoparticles Induce

Defects in Supported Lipid Bilayers. *Nano Letters* **2008,** 8, (2), 420-424.

57. Hanson, M. C.; Crespo, M. P.; Abraham, W.; Moynihan, K. D.; Szeto, G. L.; Chen, S. H.; Melo, M. B.; Mueller, S.; Irvine, D. J., Nanoparticulate STING agonists are potent lymph node–targeted vaccine adjuvants. *The Journal of Clinical Investigation* 125, (6), 2532-2546.

58. Templeton, N. S.; Lasic, D. D.; Frederik, P. M.; Strey, H. H.; Roberts, D. D.; Pavlakis, G. N., Improved DNA: liposome complexes for increased systemic delivery and gene expression. *Nat Biotech* **1997,** 15, (7), 647-652.

59. Zhu, L.; Lu, Y.; Miller, D. D.; Mahato, R. I., Structural and Formulation Factors Influencing Pyridinium Lipid-Based Gene Transfer. *Bioconjugate Chemistry* **2008,** 19, (12), 2499-2512.

60. Blume, G.; Cevc, G., Liposomes for the sustained drug release in vivo. *Biochimica et Biophysica Acta (BBA) - Biomembranes* **1990,** 1029, (1), 91-97.

61. Phanse, Y.; Carrillo-Conde, B. R.; Ramer-Tait, A. E.; Roychoudhury, R.; Pohl, N. L. B.; Narasimhan, B.; Wannemuehler, M. J.; Bellaire, B. H., Functionalization of polyanhydride microparticles with di-mannose influences uptake by and intracellular fate within dendritic cells. *Acta Biomaterialia* **2013,** 9, (11), 8902-8909.

62. Perrier, T.; Saulnier, P.; Fouchet, F.; Lautram, N.; Benoît, J.-P., Post-insertion into Lipid NanoCapsules (LNCs): From experimental aspects to mechanisms. *International Journal of Pharmaceutics* **2010,** 396, (1–2), 204-209.

63. Liu, H.; Moynihan, K. D.; Zheng, Y.; Szeto, G. L.; Li, A. V.; Huang, B.; Van Egeren, D. S.; Park, C.; Irvine, D. J., Structure-based programming of lymph-node targeting in molecular vaccines. *Nature* **2014,** 507, (7493), 519-522.

64. Mornet, S.; Lambert, O.; Duguet, E.; Brisson, A., The Formation of Supported Lipid Bilayers on Silica Nanoparticles Revealed by Cryoelectron Microscopy. *Nano Letters* **2005,** 5, (2), 281-285.

65. Tahara, Y.; Fujiyoshi, Y., A new method to measure bilayer thickness: Cryo-electron microscopy of frozen hydrated liposomes and image simulation. *Micron* **1994,** 25, (2), 141-149.

66. Gemeinhart, R. A.; Luo, D.; Saltzman, W. M., Cellular Fate of a Modular DNA Delivery System Mediated by Silica Nanoparticles. *Biotechnology Progress* **2005,** 21, (2), 532-537.

67. Tan, W.; Wang, K.; He, X.; Zhao, X. J.; Drake, T.; Wang, L.; Bagwe, R. P., Bionanotechnology based on silica nanoparticles. *Medicinal Research Reviews* **2004,** 24, (5), 621-638.

68. Luo, D.; Han, E.; Belcheva, N.; Saltzman, W. M., A self-assembled, modular DNA delivery system mediated by silica nanoparticles. *Journal of Controlled Release* **2004,** 95, (2), 333-341.

69. Zhao, Y.; Trewyn, B. G.; Slowing, I. I.; Lin, V. S. Y., Mesoporous Silica Nanoparticle-Based Double Drug Delivery System for Glucose-Responsive Controlled Release of Insulin and Cyclic AMP. *Journal of the American Chemical Society* **2009,** 131, (24), 8398-8400.

70. Trewyn, B. G.; Giri, S.; Slowing, I. I.; Lin, V. S. Y., Mesoporous silica nanoparticle based controlled release, drug delivery, and biosensor systems. *Chemical Communications* **2007**, (31), 3236-3245.

71. Weiner, G. J.; Liu, H.-M.; Wooldridge, J. E.; Dahle, C. E.; Krieg, A. M., Immunostimulatory oligodeoxynucleotides containing the CpG motif are effective as immune adjuvants in tumor antigen immunization. *Proceedings of the National Academy of Sciences* **1997,** 94, (20), 10833-10837.

72. DeMuth, P. C.; Min, Y.; Irvine, D. J.; Hammond, P. T., Implantable Silk Composite Microneedles for Programmable Vaccine Release Kinetics and Enhanced Immunogenicity in Transcutaneous Immunization. *Advanced Healthcare Materials* **2014,** 3, (1), 47-58.

73. Sun, B.; Ji, Z.; Liao, Y.-P.; Wang, M.; Wang, X.; Dong, J.; Chang, C. H.; Li, R.; Zhang, H.; Nel, A. E.; Xia, T., Engineering an Effective Immune Adjuvant by Designed Control of Shape and Crystallinity of Aluminum Oxyhydroxide Nanoparticles. *ACS Nano* **2013,** 7, (12), 10834-10849.

74. Pillarisetty, V. G.; Katz, S. C.; Bleier, J. I.; Shah, A. B.; DeMatteo, R. P., Natural Killer Dendritic Cells Have Both Antigen Presenting and Lytic Function and in Response to CpG Produce IFN-γ via Autocrine IL-12. *The Journal of Immunology* **2005,** 174, (5), 2612-2618.

75. Kozak, W.; Wrotek, S.; Kozak, A., Pyrogenicity of CpG-DNA in mice: role of interleukin-6, cyclooxygenases, and nuclear factor-κB. *American Journal of Physiology - Regulatory, Integrative and Comparative Physiology* **2006,** 290, (4), R871-R880.

76. Yi, A.-K.; Krieg, A. M., Cutting Edge: Rapid Induction of Mitogen-Activated Protein Kinases by Immune Stimulatory CpG DNA. *The Journal of Immunology* **1998,** 161, (9), 4493-4497.

77. Ballas, Z. K.; Krieg, A. M.; Warren, T.; Rasmussen, W.; Davis, H. L.; Waldschmidt, M.; Weiner, G. J., Divergent Therapeutic and Immunologic Effects of Oligodeoxynucleotides with Distinct CpG Motifs. *The Journal of Immunology* **2001,** 167, (9), 4878-4886.

78. Geary, S. M.; Lemke, C. D.; Lubaroff, D. M.; Salem, A. K., Tumor immunotherapy using adenovirus vaccines in combination with intratumoral doses of CpG ODN. *Cancer Immunology, Immunotherapy* **2011,** 60, (9), 1309-1317.

79. Suzuki, Y.; Wakita, D.; Chamoto, K.; Narita, Y.; Tsuji, T.; Takeshima, T.; Gyobu, H.; Kawarada, Y.; Kondo, S.; Akira, S.; Katoh, H.; Ikeda, H.; Nishimura, T., Liposome-Encapsulated CpG Oligodeoxynucleotides as a Potent Adjuvant for Inducing Type 1 Innate Immunity. *Cancer Research* **2004,** 64, (23), 8754-8760.

80. Wakita, D.; Chamoto, K.; Zhang, Y.; Narita, Y.; Noguchi, D.; Ohnishi, H.; Iguchi, T.; Sakai, T.; Ikeda, H.; Nishimura, T., An indispensable role of type-1 IFNs for inducing CTL-

mediated complete eradication of established tumor tissue by CpG-liposome co-encapsulated with model tumor antigen. *International Immunology* **2006,** 18, (3), 425-434.

81. Baines, J.; Celis, E., Immune-mediated Tumor Regression Induced by CpG-containing Oligodeoxynucleotides. *American Association for Cancer Research* **2003,** 9, (7), 2693-2700.

82. Gungor, B.; Yagci, F. C.; Tincer, G.; Bayyurt, B.; Alpdundar, E.; Yildiz, S.; Ozcan, M.; Gursel, I.; Gursel, M., CpG ODN Nanorings Induce IFNα from Plasmacytoid Dendritic Cells and Demonstrate Potent Vaccine Adjuvant Activity. *Science Translational Medicine* **2014,** 6, (235), 235ra61-235ra61.

83. Prausnitz, M. R.; Langer, R., Transdermal drug delivery. *Nat Biotech* **2008,** 26, (11), 1261-1268.

84. Sullivan, S. P.; Koutsonanos, D. G.; del Pilar Martin, M.; Lee, J. W.; Zarnitsyn, V.; Choi, S.-O.; Murthy, N.; Compans, R. W.; Skountzou, I.; Prausnitz, M. R., Dissolving polymer microneedle patches for influenza vaccination. *Nat Med* **2010,** 16, (8), 915-920.

85. Giudice, E. L.; Campbell, J. D., Needle-free vaccine delivery. *Advanced Drug Delivery Reviews* **2006,** 58, (1), 68-89.

86. DeMuth, P. C.; Min, Y.; Huang, B.; Kramer, J. A.; Miller, A. D.; Barouch, D. H.; Hammond, P. T.; Irvine, D. J., Polymer multilayer tattooing for enhanced DNA vaccination. *Nat Mater* **2013,** 12, (4), 367-376.

87. DeMuth, P. C.; Garcia-Beltran, W. F.; Ai-Ling, M. L.; Hammond, P. T.; Irvine, D. J., Composite Dissolving Microneedles for Coordinated Control of Antigen and Adjuvant Delivery Kinetics in Transcutaneous Vaccination. *Advanced Functional Materials* **2013,** 23, (2), 161-172.

88. Prausnitz, M. R.; Mitragotri, S.; Langer, R., Current status and future potential of transdermal drug delivery. *Nat Rev Drug Discov* **2004,** 3, (2), 115-124.

89. Liu, H.; Irvine, D. J., Guiding Principles in the Design of Molecular Bioconjugates for

Vaccine Applications. *Bioconjugate Chemistry* **2015**.

90. Weber, J.; Boswell, W.; Smith, J.; Hersh, E.; Snively, J.; Diaz, M.; Miles, S.; Liu, X.; Obrocea, M.; Qiu, Z.; Bot, A., Phase 1 Trial of Intranodal Injection of a Melan-A/MART-1 DNA Plasmid Vaccine in Patients With Stage IV Melanoma. *Journal of Immunotherapy* **2008,** 31, (2), 215-223.

91. Indermun, S.; Luttge, R.; Choonara, Y. E.; Kumar, P.; du Toit, L. C.; Modi, G.; Pillay, V., Current advances in the fabrication of microneedles for transdermal delivery. *Journal of Controlled Release* **2014,** 185, 130-138.

92. Hegde, N. R.; Kaveri, S. V.; Bayry, J., Recent advances in the administration of vaccines for infectious diseases: microneedles as painless delivery devices for mass vaccination. *Drug Discovery Today* **2011,** 16, (23–24), 1061-1068.

93. Cordeiro, A. S.; Alonso, M. J., Recent advances in vaccine delivery. *Pharmaceutical Patent Analyst* **2015,** 5, (1), 49-73.

94. Blank, I. H., Penetration of Low-Molecular-Weight Alcohols into Skin. *Journal of Investigative Dermatology* 43, (5), 415-420.

95. McAllister, D. V.; Wang, P. M.; Davis, S. P.; Park, J.-H.; Canatella, P. J.; Allen, M. G.; Prausnitz, M. R., Microfabricated needles for transdermal delivery of macromolecules and nanoparticles: Fabrication methods and transport studies. *Proceedings of the National Academy of Sciences* **2003,** 100, (24), 13755-13760.

96. Trevaskis, N. L.; Kaminskas, L. M.; Porter, C. J. H., From sewer to saviour [mdash] targeting the lymphatic system to promote drug exposure and activity. *Nat Rev Drug Discov* **2015,** advance online publication.

97. DeMuth, P. C.; Moon, J. J.; Suh, H.; Hammond, P. T.; Irvine, D. J., Releasable Layer-by-Layer Assembly of Stabilized Lipid Nanocapsules on Microneedles for Enhanced Transcutaneous Vaccine Delivery. *ACS Nano* **2012,** 6, (9), 8041-8051.

98. Naito, S.; Ito, Y.; Kiyohara, T.; Kataoka, M.; Ochiai, M.; Takada, K., Antigen-loaded dissolving microneedle array as a novel tool for percutaneous vaccination. *Vaccine* **2012,** 30, (6), 1191-1197.

99. Lee, J. W.; Choi, S.-O.; Felner, E. I.; Prausnitz, M. R., Dissolving Microneedle Patch for Transdermal Delivery of Human Growth Hormone. *Small* **2011,** 7, (4), 531-539.

100. Hauri, A. M.; Armstrong, G. L.; Hutin, Y. J. F., The global burden of disease attributable to contaminated injections given in health care settings. *International Journal of STD & AIDS* **2004,** 15, (1), 7-16.

ABSTRACT

ENHANCEMENT OF CANCER VACCINE EFFICACY VIA NANOPARTICLE OR MOLECULAR-BASED ADJUVANTS

by

MYUNGGI AN

August 2016

Advisor: Dr. Haipeng Liu

Major: Materials Science and Engineering

Degree: Master of Science

Adjuvants are immunomodulators which enhance immune responses to vaccines. However, parenteral administration of unformulated adjuvants fails to reach lymph nodes (LNs), the anatomic organ where the primary functions of immune cells are orchestrated. The LN-targeting delivery plays the key roles in promoting immune activation and has the great potential to transform disease treatment. The main goal of this thesis is to develop efficient vaccine delivery systems to target therapeutics into draining lymph nodes (dLNs) for ensuring their immunostimulatory activity. We introduced therapeutic applications of activating TLR9 with synthetic CpG oligodeoxynucleotide (ODN) agonists in nanoparticle or molecular form to activate immune responses in animal models. As a nanoparticle deliver platform, positively charged silica nanoparticles (SiNPs) were explored to load immunomodulators that are capable of targeting dLNs and mimicking the size, geometry and surface feathers of live viral pathogens. Immunization with nanoparticles showed potent cellular and humoral immunity superior to vaccination with soluble CpG ODNs.

We next explored the transdermal delivery platform using dissolving microneedle arrays (MNs), which can penetrate the skin and facilitate the rapid release of vaccine components in epidermis. We combined this strategy with an albumin ‘hitchhiking’ approach that can promote

interaction with and uptake across the lymphatic endothelium. Vaccination via MNs generated robust immune responses, showing enhanced T cell and antibody responses. We characterized the morphology and vaccine loading capabilities of MNs, and systematically explored how the transdermal delivery of molecular vaccines impacted cellular and humoral immunogenicity. We expect that the results of our work will contribute to the advancement of vaccine delivery systems and will help to develop more efficient therapeutics for treating disease or cancer.

AUTOBIOGRAPHICAL STATEMENT

EDUCATION

M.S., Energy and Environmental Engineering, Korea University of Science and Technology, August 2013

B.S., Materials Chemistry and Engineering, Konkuk University, February 2011

PUBLICATIONS

1. **M. An**, H. Y. Ha, "Facile one-step and template-free synthesis of hollow carbon fibers and its application to catalyst support for direct methanol fuel cells", submitted.
2. **M. An**, A. Mehmood, H. Y. Ha, "Analysis of the crossover behaviors of methanol and CO_2 in direct methanol fuel cells: Comparison of Nafion and hydrocarbon-based membranes", submitted.
3. A. Mehmood, **M. An,** J. Hwang, H. Y. Ha, "Improving DMFC performance through structural modification of cathode catalyst layer", submitted.
4. **M. An**, A. Mehmood, H. Y. Ha, "A novel sensor-less methanol concentration control method for direct methanol fuel cells through feedback from the amplitude of voltage fluctuation", Energy, 100 (2016) 217-226.
5. A. Mehmood, M. A.Scibioh, J. Prabhuram, **M. An**, H. Y. Ha, "A review on durability issues and restoration techniques in long-term operations of direct methanol fuel cells", Journal of Power Sources, 297 (2015) 224-241.
6. **M. An**, A. Mehmood, H. Y. Ha, "A sensor-less methanol concentration control system based on the feedback of stack temperature", Applied Energy, 131 (2014) 257-266.
7. A. Mehmood, **M. An**, H. Y. Ha, "Physical degradation of cathode catalyst layer and accelerated water flooding in long-term DMFC operation", Applied Energy, 129 (2014) 346-353.
8. **M. An**, A. Mehmood, H. Y. Ha, "Sensor-less control of the methanol concentration of direct methanol fuel cells at varying ambient temperatures", Applied Energy, 129 (2014) 104-111.
9. D. S. Jeong, H. W. Ahn, S. D. Kim, **M. An**, S. Lee, B. Cheong, "Numerical study on passive crossbar arrays employing threshold switches as cell-selection-devices", Electronic Materials Letters, 8 (2012) 169-174.